catalysts

MDPI

Review

Recent Combinations of Electrospinning with Photocatalytic Technology for Treating Polluted Water

He Lv [1], Yanan Liu [1], Yubin Bai [1], Hongpu Shi [1], Wen Zhou [1], Yaoning Chen [1], Yang Liu [2] and Deng-Guang Yu [1,*]

[1] School of Materials and Chemistry, University of Shanghai for Science and Technology, 516 Jungong Road, Shanghai 200093, China
[2] School of Chemistry and Chemical Engineering, Shanghai University of Engineering Science, 333 Long Teng Road, Shanghai 201620, China
* Correspondence: ydg017@usst.edu.cn

Abstract: Dyes, antibiotics, heavy metal ions, and bacteria are important sources of water pollution. How to solve these issues has become a problem in the fields of science and technology. People have developed a variety of technologies to treat pollutants in water. Photocatalytic technology came into being. As a simple and environmentally friendly treatment technology, it has been widely studied by the scientific community. Traditional powder photocatalysts cause secondary pollution to the environment and are not conducive to recycling. Therefore, large specific surface area and reusable membrane photocatalysts built by electrospinning technology have become a favorite of today's scientific community. Nanofiber membranes prepared by electrospinning technology have a variety of structures, which can meet the needs of different occasions. This review summarizes and discusses research progress in electrospinning technology, the relationship between the structure and treatment of electrospun fiber membranes, and their impacts on the photocatalytic performance of nanofiber membranes. The performance, challenges, and future development directions of nanofiber membranes with different structures, prepared by different kinds of electrospinning techniques using photocatalysis to treat different pollutants, are reviewed.

Keywords: electrospinning technology; photocatalytic technology; polluted water; nanofibers; nanostructures; composites

Citation: Lv, H.; Liu, Y.; Bai, Y.; Shi, H.; Zhou, W.; Chen, Y.; Liu, Y.; Yu, D.-G. Recent Combinations of Electrospinning with Photocatalytic Technology for Treating Polluted Water. *Catalysts* **2023**, *13*, 758. https://doi.org/10.3390/catal13040758

Academic Editors: Juan José Rueda-Márquez, Javier Moreno-Andrés and Irina Levchuk

Received: 31 January 2023
Revised: 4 April 2023
Accepted: 12 April 2023
Published: 15 April 2023

1. Introduction

With the development of global industrialization and the rapid growth in population, the problem of environmental pollution has become increasingly prominent. The environment is heavily threatened by poisonous and dangerous contaminants, which pose a severe threat to human existence and growth [1]. Water contamination has become a significant contributor to declining public health. Wastewater from a variety of sources, including landfill leachate, domestic sewage, hospital sewage, industrial, and agricultural sewage discharge, among others, may infiltrate surface water and groundwater environments directly or indirectly [2,3]. How to solve these problems has become a primary consideration for socially sustainable development. Conventional treatment technologies include physical, chemical, and biological technologies [4–6]. However, some pollutants in water have stable chemical properties and strong toxicity, and these treatment technologies can not completely treat them, instead converting them into another form of pollutant [7]. Thus, it is problematic to use these technologies for treatment.

Therefore, photocatalytic technology came into being. Photocatalytic technology [8,9] is the preferred option in water treatment due to its benefits of low energy consumption, gentle reaction conditions, and non–toxicity products. Under certain conditions, pollutants that are difficult to treat by ordinary methods and have strong toxicity can be oxidized by high reactivity hydroxyl radicals (•OH), superoxide radicals ($\bullet O_2^-$), and holes (h^+),

with oxidation to CO_2, H_2O, and other inorganic substances or small molecular substances with low toxicity and easy degradation [10]. There are two conditions for generating a photocatalytic reaction: (1) illumination and excitation from various energy sources; (2) the material contains semiconductor photocatalysts. When a semiconductor photocatalyst is excited by an energy source, electrons on the valence band of the semiconductor are excited to the conduction band, leaving holes on the valence band. The formed electrons and holes react with water molecules and oxygen to generate active radicals, which can react with pollutants in water, ultimately forming non–toxic products, such as water and carbon dioxide [11]. Although photocatalysis has developed rapidly in recent years, few photocatalysts stand out in real–world applications due to their weak photocatalytic efficiency and recycling durability. The majority of photocatalysts are available as powders [12,13]. Powder photocatalysts not only lump readily, losing the activity centers, but are also difficult to separate and recycle from water. Most significantly, if the photocatalyst has not yet fully reacted, the toxicity of the photocatalyst and other pollutants will also be greater. In addition, powdered photocatalysts are prone to aggregation, and may quickly and readily cause health hazards by entering the body through the respiratory system.

In order to overcome the shortcomings of powder photocatalysts, many carriers have been developed to immobilize powder photocatalysts, including photocatalytic membranes [14]. The photocatalytic membranes can improve the recycle photocatalytic rate and reduce the toxicity of powder photocatalysts. Most importantly, loading photocatalysts onto electrospun NF membranes provides new solutions for photocatalytic technology to degrade pollutants in wastewater. Due to the load, large specific surface area, and high porosity of electrospun NFs, they can stabilize the material structure, provide more reactive sites, and improve the separation efficiency of photogenerated carriers. Photocatalytic membranes, such as polyacrylonitrile (PAN) [15], cellulose acetate (CA) [16], and poly(vinylidene fluoride) (PVDF) [17] membranes have been prepared to degrade pollutants. However, traditional photocatalytic membranes are obtained by coating or mixing photocatalysts in the membrane and then pouring [18] or spin coating [19]. Compared to powder photocatalysts, these technologies can severely limit the efficiency of photocatalytic membranes; the photocatalysts coated on the surface of the membranes can exhibit aggregation, which can significantly reduce the photocatalytic efficiency [20]. After several cycles, the photocatalyst on the surface is prone to fall off due to poor adhesion. The photocatalyst doped in the photocatalyst membrane is trapped inside the membrane, resulting in a decrease in the degradation efficiency of the photocatalyst. Membrane carrier materials may age under the action of light and degrade, which can decrease the mechanical stability of the material. Powdered photocatalysts in the membrane are also prone to agglomerate, resulting in pore clogging of the membrane, which not only reduces the separation efficiency of electrons and holes but also reduces the active sites of the photocatalytic reaction. Therefore, it is crucial to develop a new type of photocatalyst. Photocatalytic membranes [21,22] are regarded as a vital avenue for innovation and sustainable development since they are effective and simple to recover. In addition, compared with powder materials, membranes are easier to recover and have a stable structure, suggesting great potential in the treatment of pollutants in water using photocatalytic technology.

Electrospinning technology [23–25] is a simple and convenient technology to prepare membrane materials. Membrane materials prepared by electrospinning technology [26–28] retain the stability of the material structure after treatment. These materials are widely used in various fields, such as environmental remediation, food preservation, drug release, multifunctional materials, hydrogen evolution reaction performance, electronic devices, etc., [1,29–36]. Due to their high surface area and ease of retrieval, which are favorable to the photocatalytic activities required to remove pollutants from water, nanofibrous structures have significant potential for this task. Electrospinning is a potent technique for different morphologies and structure fibers [16,20,31] that are appropriate for use in tissue engineering, biological materials, and air and water filters. The nonwoven nature of the nanofibers (NFs), in particular, makes it easier to remove contaminants from water

effectively. This research area is very active, with an increasing number of scientific articles published each year (Figure 1). In 1997, Martin et al. initially proposed electrospun NFs for the photocatalytic degradation of pollutants [37]. Then, the first research on electrospun NFs for photocatalytic degradation of pollutants appeared in 2003 [38], and research on electrospun NFs has increased year by year (Figure 1). Uniaxial nanofiber (NF) membranes, porous NF membranes, coaxial NF membranes, Janus NF membranes, and multi–fluid electrospun fiber membranes gradually appeared [20]. Uniaxial NFs have the advantage of simple preparation and are widely used for the photocatalytic degradation of pollutants in water. However, due to the difficulties associated with the electrospinning of polymers, solvents, and photocatalysts, the mechanical properties and structure, and the easy combination of e^- and h^+ of uniaxial NFs, multi–fluid electrospinning came into being. Nanofiber membranes with special structures prepared by multi–fluid electrospinning can solve the above problems. Importantly, electrospun nanofiber membranes with different morphology and structure prepared by electrospinning technology have a good photocatalytic effect. The mechanical properties are also improved compared with uniaxial electrospun fiber membranes. Multi–fluid electrospinning technology [1,16,20,39] can be compatible with polymers with different properties, it can be used to prepare the NF membranes with stronger photocatalytic performance, better mechanical properties, higher secondary recovery. The aim of this review is to introduce progress in research relating to electrospinning technology and the use of different methods to treat electrospun nanofiber membranes, focusing on the influence of the structure and morphology of electrospun nanofiber membranes after treatment on their photocatalytic performance. In addition, this review also considers the impact of electrospun nanofiber membranes on the photocatalytic degradation performance of different pollutants, and discusses the impact, challenges, and future development directions of nanofiber membranes with different structures prepared by different electrospun technologies on photocatalytic performance, and provides guidance for research in this field.

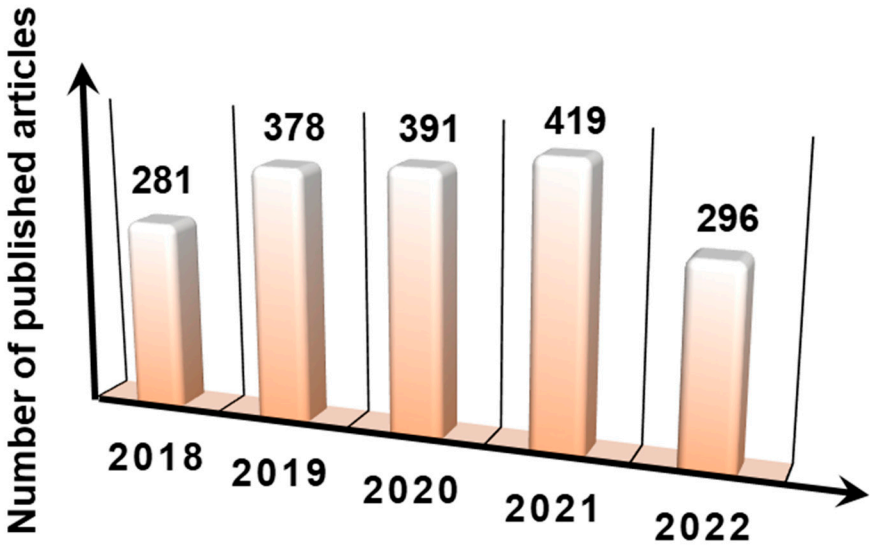

Figure 1. According to the Web of Science database, the number of papers published during the past five years. "electrospinning or NFs" and "photocatalysis or photocatalyst" were the keywords used for the Title/Abstract section. (https://www.webofscience.com, accessed on 29 January 2023).

2. The Most Recent Developments in Electrospinning

2.1. The Electrospinning Process

Electrospinning technology, abbreviated as "electrospinning", is a technology that uses polymer fluids to obtain nano- or micro-fibers by pulling under a strong electric field. The electrospinning process refers to a syringe being filled with the solution, and the formation of a droplet at the tip of the needle under the action of surface pressure. When the voltage is

turned on, the droplets form the shape of a cone as a result of the action of the high–voltage electric field. At the same time, the small droplets are mutually rejected by the surface tension and the surface charge [40]. The direction of these two forces is opposite. When the electric field power and the surface tension are equal, the small liquid droplets reach balance and the half–cone angle is 49.3°, which is the Taylor cone. When the strength of the electric field exceeds the surface tension, the top of the Taylor cone forms a fine flow spray (liquid fiber bundle). In the process of leaving the spraying head, the material passes through a series of unstable stretching, splitting, and refinement phases during the migration of the collecting board. The solvent on the surface of the fiber beam continues to volatilize (or undergoes melt cooling and solidification). Finally, the fiber falls onto the collecting board [40]. The process of electrospinning is shown in Figure 2.

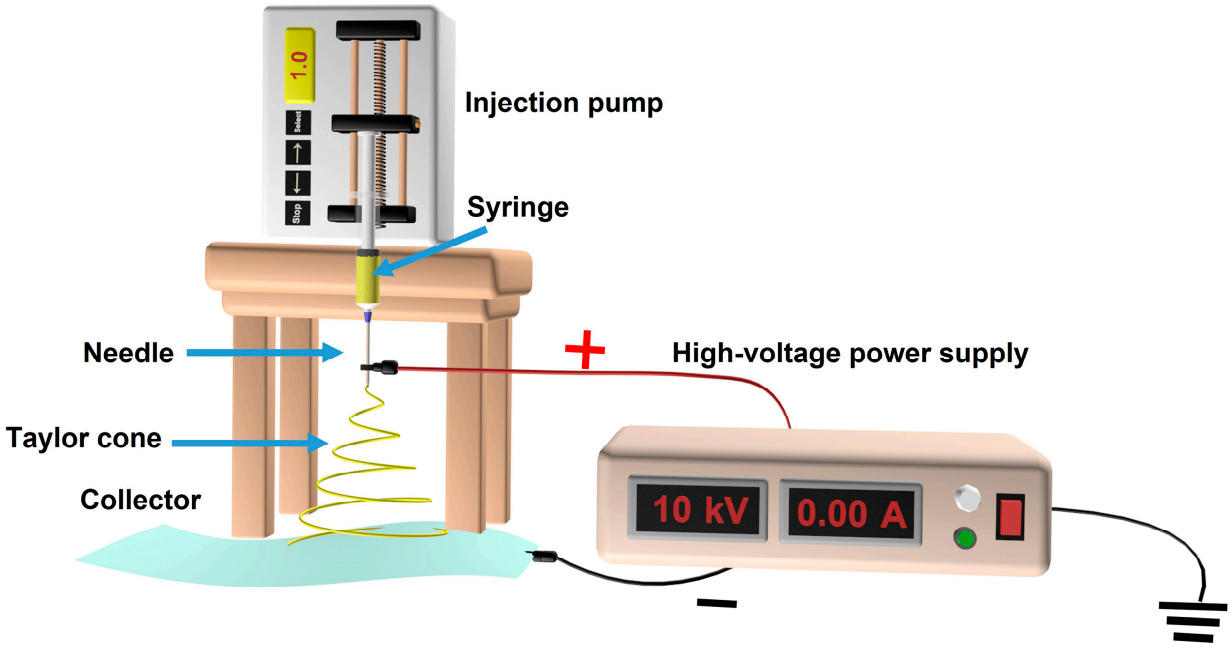

Figure 2. Schematic diagram of the electrospinning devices.

2.2. The Devices and Processing Parameters of Electrospinning

The devices used in the electrospinning process are divided into the following types: electrostatic generators, syringes, pushing pumps, and receivers [41]. Traditional electrospinning generators are positive poles [23]. Negative high–voltage electrospinning generators have been developed in recent years, which are often used in conjugated electrospinning [42], as shown in Figure 3a. The electrospinning fluid in the two spinnerets can overcome surface tension and viscous forces to spray out, generating numerous NFs with positive and negative charges under the influence of positive and negative high–voltage direct–current (DC) power supplies. At the two nozzles, a significant quantity of positive and negative charges assemble to create an electric field. In Figure 2, the red dot dotted region indicates the direction of the electric field lines. Using conjugated electrospinning, Janus NFs can be easily prepared, but the components of the NFs do not interact with each other at the same time. However, due to the interference of electric charges and other factors in the air, the yield of Janus NFs is relatively low. In addition, alternating current (AC) electrospinning generators [43] (Figure 3b) and low–voltage electrostatic generators [44] (Figure 3c) have gradually appeared. The fibers prepared by AC electrospinning technology are positively charged and react negatively to polarity changes; unlike DC rotation, they do not need opposing electrodes. Under the electric field, the formed fibers are pulled in the opposite direction, the NFs are transferred from the electrode, and are dragged toward the existing fibers by charge effects. Low–voltage electrospinning is relatively safe. However,

its application range is relatively narrow, and it can only prepare some polymers to form fibers easily. Due to the relatively low voltage, the molecular stretching in the fibers is not sufficient and the morphology of fibers varies. The most widely used method involves a high–voltage positive electrostatic generator [45] due to its safety, stability, and yield. A more stable surface charge (+) distribution of the polymer jet can be generated by positive high–voltage electricity, with the charges (−) carried by the receiver. NFs prepared by positive high–voltage electrospinning have a uniform diameter distribution, more diverse morphology, and are produced in greater yield.

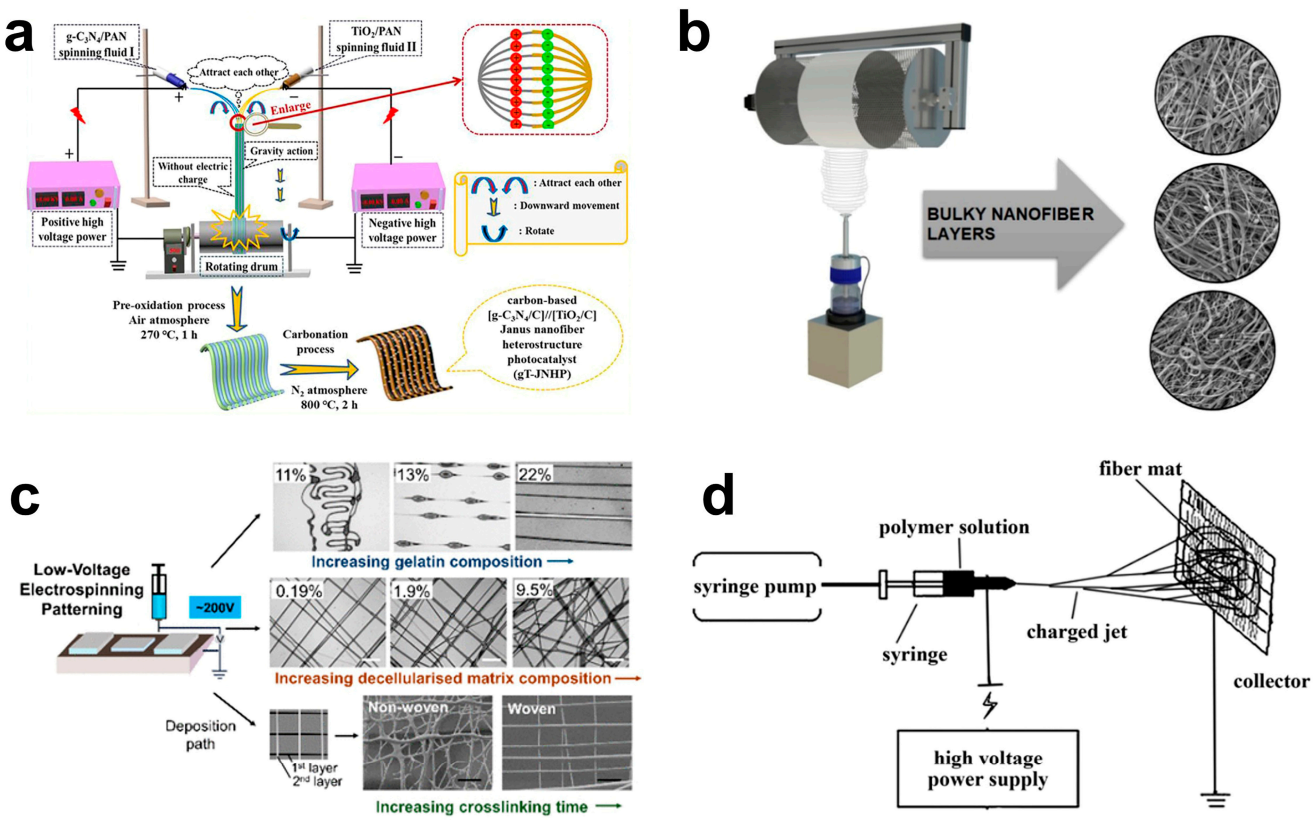

Figure 3. Diagram of conjugated electrospinning set–up (**a**) [42], Copyright 2022, Wiley. Diagram of AC electrospinning set–up (**b**) [43], Copyright 2019, American Chemical Society. Diagram of low–voltage electrospinning set–up (**c**) [44]. Diagram of positive high–voltage electrospinning devices set–up (**d**) [45], Copyright 2011, Elsevier.

The syringe is generally made from plastic. The needles are of two types: stainless–steel needles and plastic needles [43]. The types of receivers are wire mesh and tin foil, which are developed for the roller [42], turntable [46], and liquid–phase receiving devices [47]. Different kinds of receivers greatly enrich the types and performance of NF membranes. The wire mesh, tin foil, and liquid–phase receivers are used to receive the uniform NFs membrane. The orderly aligned nanofiber membrane can be prepared using a roller and turntable. Typically, some NFs that cannot be fully dried are collected using liquid phase technology during the electrospinning process; the obtained nanofiber membranes have better performance.

Factors affecting electrospinning include systemic factors and the electrospinning process parameters.

Systemic factors include the polymer type, solution concentration [48], and solvent type [49]. Polymers selected for the preparation of electrospun NFs were initially mainly polyvinylpyrrolidone (PVP) [50], PAN [51], PVDF [33], methyl polyacrylate (PMMA) [31], polyvinyl alcohol (PVA) [52], polystyrene (PS) [53] or other organic polymers [54] that were easy to spin. Organic polymers have been developed into biocompatible polymers, such

as collagen [55], polylactic acid [56], gelatin [57], chitin [58], chitosan [58], and sodium alginate [59]. Some inorganic materials and non–spinnable materials [39] are also added. Adding polymers which are easy to electrospin into some non–spinnable polymers can enhance the spinnability of NFs [17]. At the same time, different kinds of polymers will undergo phase separation [60]. Compared with NFs prepared by a single kind of polymer, NFs prepared using a variety of polymers will have different morphologies, and their performances will also be improved [17]. In addition, NFs membranes with different morphologies can also be prepared using different solvents, water–soluble polymers, and salts. The principles for selecting polymers are related to the polymer types, the solvent volatility, the compatibility between the solvent and the polymer, and the interaction between the solvent and the polymer molecular chain. Highly volatile solvents and solvents with less interaction with molecular chains can enable preparation of NFs with a smaller diameter. In addition, all electrospinning solutions have spinnable concentrations; the electrospinning solution is sprayed out in the form of droplets or beads below the appropriate concentration. Above this concentration, the concentration is too high, and achieving flow of the electrospinning fluid is difficult, which will hinder the electrospinning process. The types of solvents initially used in electrospinning were mostly single organic solvents. Today, most solvents used are multiple organic solvents, which enable preparation of a variety of NF membranes with different appearances and properties [61,62]. The solvents used for electrospinning are mainly divided into two categories: one category is volatile solvents, such as chloroform and acetone [63,64]; the other category is non–volatile solvents, such as water, ethanol [63,64], and so on. By combining different volatile organic solvents, NF membranes with different morphologies can be prepared. For example, porous NFs can be prepared by mixing acetone and DMF [65]. Because acetone is volatile, holes will appear on the fiber surface; the relatively weak volatility of DMF plays a role in maintaining the fiber morphology. Solvents can also be divided into good solvents and poor solvents according to their solubility. The molecular chain structure of polymers can be stretched in good solvents, while poor solvents are not easy to stretch. The structural differences caused by mixing these two kinds of solvents can easily cause local defects in the polymer, resulting in different morphologies and pore structures on the NFs [66].

The electrospinning process parameters include the electric field strength and receiving distance, which are important parameters affecting the performance of NF membranes [67]. The applied electric field strength generally increases with increase in the electric field strength. At the same time, a high electric field strength enables greater acceleration of the jet. These two factors can cause the electrostatic stress of the jet to increase, increasing the tensile rate, which is conducive to the preparation of finer fibers. If some conductive solutions are added appropriately to the spinning solution to improve the conductivity, finer fibers can be prepared. The relationship between the distance between the needle and the receiver is important: if the spinning distance is too close, the solvent will be too slow to volatilize, and the fibers will tend to bond with each other; if the spinning distance is too large, the filaments will not be easy to collect on the receiver due to weakening of the electric field strength. With increase in the receiving distance, the fiber diameter decreases.

In addition, environmental factors, such as the humidity and temperature, can also affect the morphology of fibers. For example, Liu et al. [68] found that adjusting the relief temperature can affect the polymer's annual and solvent evaporation rate during electrospinning, thereby affecting the diameter and morphology of the fiber. Liu et al. [69] have shown that suitable humidity can enable preparation of NFs with better morphology. As indicated above, many factors can affect the electrospinning process, enabling preparation of NFs with different morphologies and functions. The effects of varying factors, provides a theoretical basis for the preparation of NF membranes with excellent photocatalytic properties.

2.3. Types of Nanofibers Prepared by Electrospinning Technology

Prototype of electrospinning technology include uniaxial NF [70], coaxial NF [71,72], and Janus NF [73], as shown in Figure 4. In the 16th century, William Gilbert identified the

electrostatic force in liquids, which underpinned the development of electrospinning [74]. The simplest approach is the uniaxial electrospinning technique, as shown in Figure 2. In uniaxial electrospinning technology, only a single fluid is involved; the compositions of solvents, polymers, and functional particles are relatively simple, without considering the impact of other factors. Uniaxial electrospinning technology is simple, easy to operate, and the prepared membranes have stable structure and high yield, which is beneficial for further surface functionalization, heat treatment, and hydrothermal growth of functional particles.

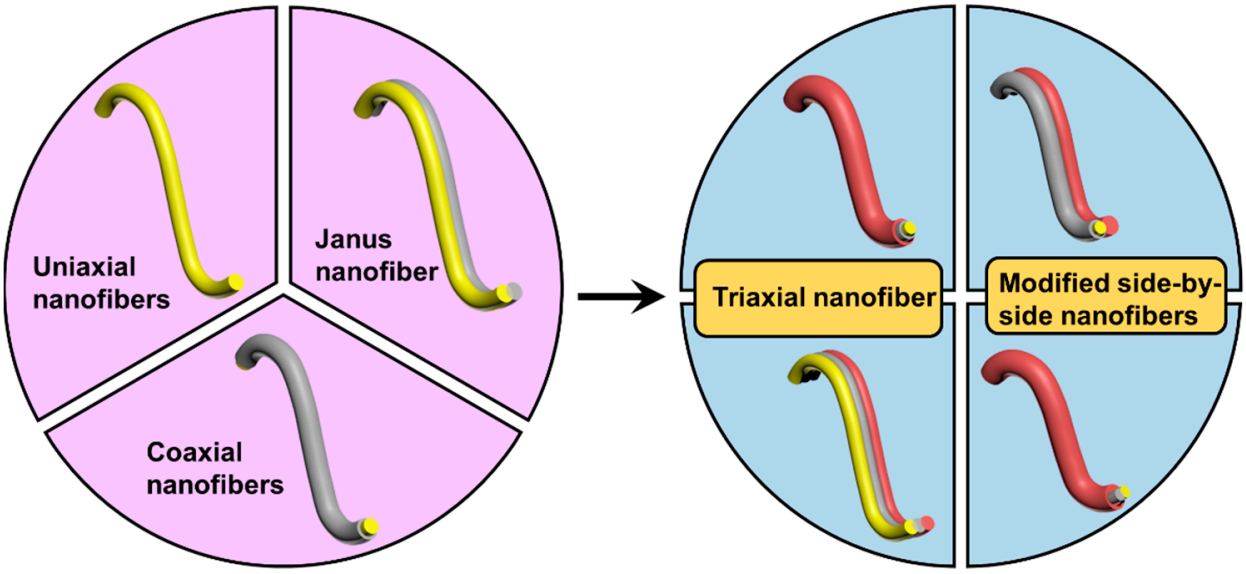

Figure 4. Diagram showing recent developments in electrospinning.

In 2003, coaxial electrospinning technology was established to manufacture core–shell nanofibers with varied material properties [75]. Two different kinds of polymers can be combined using coaxial electrospinning technology to create core–shell micro– or nanofibers. The ability of coaxial electrospinning to prepare core–shell structured fibers has attracted increasing attention because it can enhance the properties of the materials for a variety of applications, particularly for environmental purification. The coaxial electrospinning technique is anticipated to be able to prevent the mixing of the polymers that make up the core and the shell. Additionally, this technology offers superior mechanical characteristics, porosity, and hydrophilicity, and minimizes membrane swelling. The synergistic effect created by the two distinct polymers can compensate for the weakness of one of the polymers.

Uniaxial NFs [70] and coaxial NFs have the advantages of simple operation and easy preparation. However, the demands of people have increased with the development of society, so there is a need to introduce particles and polymers with different functions to enhance the performance of NF membranes. However, the addition of some non–spinning polymers and functional particles increases the difficulty of electrospinning. In addition, in order to achieve required multifunctional and mechanical properties, improvements in multi–fluid electrospinning [16,54] were developed. Improved multi–fluid electrospinning includes: (1) Triaxial NF membranes, which can enhance the multifunctional ability of the membrane and divide different functional particles into different areas. The division of functional areas can avoid the adverse effects of different types of particles. It contributes to enhancing the functions of a single function area [75]; (2) Three–level coaxial NF membranes. This structure is developed based on coaxial NFs. After adding the working solution fluid, the electrospinning performance of the polymer and particles can be greatly improved [76]. (3) Modified side–by–side electrospinning NF membranes. These can mainly be divided into two types: one type involves changing the side of the Janus NF into a coaxial NF, with the aim of it dividing the working area [77]; the other type involves adding the working

fluid to the outside of the Janus NF membrane, which can increase the spinnability of the Janus NF.

3. Treatment of Membrane

3.1. Modification of Electrospinning Membrane

3.1.1. Surface Modification

In order to improve photocatalytic degradation activity, moderately inert polymer NFs are treated with compounds that have reactive functional groups, such as amines, carboxyls, hydroxyls, or nitriles. Typically, NF materials are submerged in an alkaline liquid to produce hydroxyl or carboxyl groups on their surface so the surface of the NF membrane can be altered to improve the interaction or deposition of photocatalyst particles.

Mohamed et al. [78] studied the photocatalytic degradation performance of a surface–modified PAN NFs/biosilica composite membrane, as depicted in Figure 5a. The PAN NF membrane was prepared by electrospinning technology. As shown in Figure 5b–d, the NF membrane contained porous diatomite and rice husk which were cross–linked. The photocatalytic performances of these membranes for the degradation of malachite green (MG) were compared. The results showed that the photocatalytic degradation efficiency of diatomite and rice straw silica membranes for MG could reach 99% after 15 and 25 min, respectively. The degradation efficiency was highest at pH = 7. Under optimal conditions, the material was able to degrade 98% of MG within 10 min. The prepared NF membrane can be used in a continuous operating mode.

A PAN NF membrane [79] was placed in solution with hydroxylamine hydrochloride and sodium hydroxide to aminate the membrane (AO–PANNM). After that, AO–PANNM was thoroughly washed and dried. The obtained AO–PANNM was put in the solution with copper sulfate and iron chloride to prepare a copper–iron bimetal modified PAN NF membrane (BM–PANNM), as shown in Figure 5e; the NFs became thinner, but their morphologies were intact (Figure 5f,g). BM–PANNM has a superfine fiber diameter (600 nm) and a large surface area (5.34 m^2 g^{-1}). It exhibits significant photocatalytic activity (>99.99%) against Active Blue 19, Active Red 195, and Acid Orange 7 within 60 min, and it has good cycle performance. This kind of modified PAN NF membrane can provide a broader platform for the degradation of dyes by NF materials in the future.

Through surface modification with hydrazine hydrate (HH) and hydroxylamine (HA) (HA–n–PAN, HH–n–PAN), and subsequent coordination with Fe^{3+}, a series of Fe–complexed PAN NF membranes (Fe–M–n–PANs) were prepared [80]. They were able to significantly improve the adsorption and photocatalytic degradation properties of azo dyes under visible light in water, as exhibited in Figure 5i–k. The higher removal efficiency was mainly due to the synergistic effect of adsorption and photocatalytic degradation in the presence of H_2O_2. In addition, the removal efficiency was determined by the ratio of HA to HH. The membrane modified with HA and HH simultaneously had higher removal efficiency than the membrane modified with a single solvent, because more active sites can be produced using HA and HH at the same time, accelerating the removal of dyes. Fe–M–n–PANs were found to enable rapid degradation of dye molecules and to free up adsorption sites for the surface to adsorb dye molecules (Figure 5h); the Fe–M–n–PANs had good cycle stability and were able to maintain excellent photocatalytic performance after five cycles. This study provides a new direction for the treatment of industrial wastewater in the future.

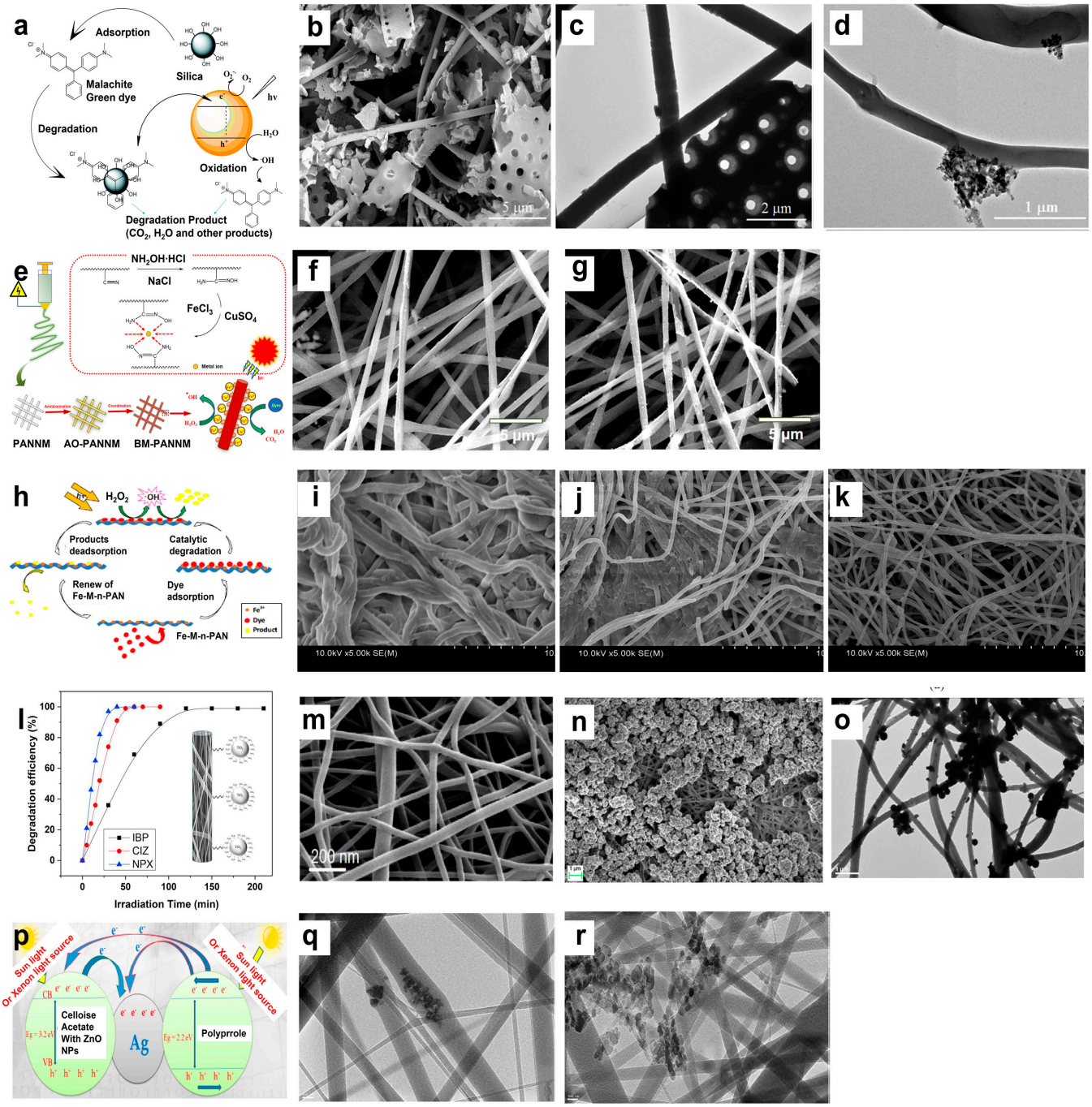

Figure 5. MG photodegradation mechanism (**a**), SEM image (**b**), TEM images (**c**,**d**) of diatomite porous microparticles on the surface of the NFs [78], Copyright 2019, Elsevier. Scheme of the design, processing, and photocatalytic degradation mechanism of BM–PANNM (**e**), SEM images of PANNM (**f**), BM–PANNM (**g**) [79], Copyright 2020, Elsevier. Schematic of removal of azo dyes from water using Fe–M–n–PAN in the presence of H_2O_2 (**h**), FE–SEM images (the plotting scale: 10 μm) of HA–n–PAN (**i**), Fe–M–n–PAN (**j**), HH–n–PAN (**k**) [80], Copyright 2017, Elsevier. The photocatalytic degradation efficiency of PAN–CNT/TiO_2–NH_2 NFs (**l**), SEM images of PAN–CNT (**m**), PAN–CNT/TiO_2–NH_2 (the plotting scale: 1 μm) (**n**), and TEM image of PAN–CNT/TiO_2–NH_2 NFs composite (the plotting scale: 1 μm) (**o**) [81], Copyright 2019, Elsevier. Diagram of the photocatalytic degradation mechanism of malachite green dye (MG) on ZnO composite NF immobilized with silver (**p**), TEM images (the plotting scale: 100 nm) of ZnO composite NF before silver immobilization (**q**), and after silver immobilization (**r**) [82].

UHeida et al. [81] added modified titanium dioxide (TiO_2) nanoparticles (NPs) to PAN/multi–walled carbon nanotube composite NFs (PAN–MWCNT/TiO_2–NH_2) and evaluated the photocatalytic degradation performance of PAN–MWCNT/TiO_2–NH_2 for ibuprofen, cetirizine, and naproxen. Comparing Figure 5m with Figure 5i, it can be observed that amino–functionalized TiO_2 NPs were distributed on the surface of PAN–CNT NFs (PAN–MWCNT/TiO_2–NH_2), and the NFs were cross–linked. Examining the TEM image (Figure 5n), it can be seen that amino–functionalized TiO_2 NPs were successfully attached to the surface of PAN–CNT NFs. Because the PAN–MWCNT/TiO_2–NH_2 composite NF membrane has a large specific surface area, multiple catalytic sites, and good flexibility, it exhibited excellent photodegradation efficiency for ibuprofen, naproxen, and cetirizine. In addition, the effect of the pH value on the photocatalytic degradation efficiency was also studied; it was found that the photocatalytic degradation efficiency was highest at pH = 2–4. The NF membrane has very wide application potential in the highly efficient photocatalytic degradation of pollutants.

A high–efficiency, environment–compatible, and porous silver surface–modified photocatalytic zinc oxide/cellulose acetate/polypyrrole (ZnO/CA/Ppy) hybrid NF membrane [82] was prepared. The effects of the flow rate, applied voltage, and other electrospinning parameters were also studied. Adjusting various electrospinning parameters enabled preparation of a ZnO/CA/Ppy composite NFs with uniform morphology; the distance between the needle tip and collector was 18 cm, the CA polymer concentration was 16%, the electrospinning flow rate was 0.2 mL/h, and the applied voltage was 18 kV. Depositing Ag NPs on the ZnO/CA/Ppy composite NFs enabled production of NFs with a narrower band gap, so the photocatalytic efficiency of composite NFs could be improved (Figure 5p). The results showed that ZnO NPs were uniformly distributed on the NF membrane (Figure 5q), and ZnO/CA/Ppy/Ag composite NFs were formed after Ag NPs were deposited (Figure 5r). The photocatalytic degradation efficiency of the ZnO/CA/Ppy/Ag composite NFs was 30% higher than that of the ZnO/CA/Ppy composite NFs.

3.1.2. Pore–Making Treatment

The pore–forming treatment of NF membranes is also an important means to improve photocatalytic performance. Based on NF membranes, many improvements have been achieved using different pore–making technologies, such as post–treatment technology [83],direct technology [84], solvent technology [85], thermal treatment technology [86], etc. The porous structure of MIL–88A/PAN nanoporous membranes is enhanced by porous MIL–88A material [84]. Ag_3PO_4/P25 composite bi–polymer NF membrane were synthesized by two different polymers PMMA and PVP through post–treatment [87]. Lv et al. [83] used post–treatment technology to prepare dimethylglyoxime (DMG)/TiO_2/PAN NF mats (WS6), as shown in Figure 6. PVP was able to be removed in hot water because of the water solubility of PVP; the surface of the remaining PAN membrane appeared to have vacancies occupied by PVP (Figure 6a). An innovative porous WS6 prepared by electrospinning technology was used to deal with Ni^{2+} and methylene blue (MB) mixture pollutant treatment. Due to the capacity of DMG for detecting Ni^{2+}, the red and virgulate $Ni(DMG)_2$ that formed on the surface of NFs showed that the complex had observable adsorption capacity. The MB degradation efficiency of WS6 was 97% within 60 min, which is the most crucial factor. Most importantly, the e^- and hole (h^+) transmission paths were shortened through the porous structures. These functional NF mats may have potential application in sensing, Ni^{2+} adsorption, and the photocatalytic degradation of organic pollutants via the intermediate $Ni(DMG)_2$ as a photocatalyst. The enhanced degradation mechanism of WS6 is depicted in Figure 6b. When the heterojunction is built, an electric field is created at the interface between $Ni(DMG)_2$ and TiO_2 to encourage the accelerated flow of e^- and h^+. Inside the mat, $Ni(DMG)_2$ and TiO_2 is able to absorb ultraviolet light to produce e^- and h^+. The excited e^- in the CB of $Ni(DMG)_2$ leaps onto the CB of TiO_2. Under the action of the electric field, some of the h^+ in TiO_2 migrates to the VB in $Ni(DMG)_2$ at the same time. As a result, e^- and h^+ are separated. $\bullet O_2^-$ radicals can be created when the e^- on CB

reacts with oxygen. Water and the h^+ on VB may combine to create •OH radicals. These two varieties of radicals can oxidize MB. Small molecules, such as water and CO_2, can be produced after the degradation of MB molecules. This work successfully integrates the photocatalytic degradation of organic contaminants and metal ion adsorption. Porous NF membranes prepared by post–treatment technology can not only shorten the path of electrons and holes, but also provide more sites for photocatalytic reactions. However, this membrane has the disadvantage of easy recombination of e^- and h^+ and poor mechanical properties. How to solve this problem should be a future direction of research.

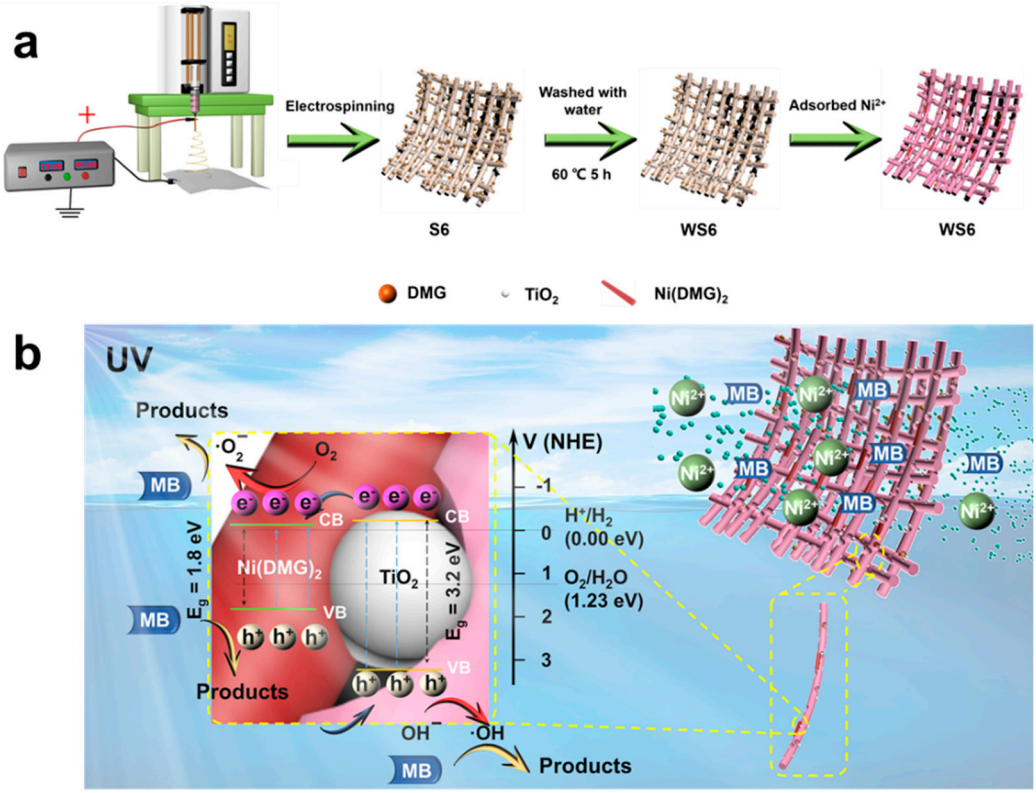

Figure 6. Schematic of preparing nanofibrous mats process (**a**) and photocatalytic degradation of MB on $Ni(DMG)_2/TiO_2$ nanofibrous mats (**b**) [83]. Copyright 2022, Elsevier.

3.2. Thermal Treatment

Heat treatment [88] of inorganic materials can change their morphology, physical structure and enhance their strength and crystallinity [89,90]. Researchers have paid a lot of attention to the preparation of inorganic NF membranes [91] because of their excellent mechanical and thermal stability [92]. Organic membranes are easily broken down under light in photocatalytic degradation [93]. Heat treatment is carried out to enhance their properties, such as wettability, mechanical capabilities, thermal characteristics, and pore size distribution. Generally, NF membranes are heated through calcination, carbonization, and hydrothermal treatment.

3.2.1. Calcination

The process of heating materials to a high temperature in a controlled atmosphere is referred to as calcination. In order to increase the mechanical and thermal stability of inorganic or ceramic materials, calcination is typically utilized.

Singh et al. [94] used *N*, *N*–dimethylformamide (DMF), zinc acetate, PAN, and ZnO to prepare porous ZnO NF by uniaxial electrospinning. Figure 7a,b show the morphologies of porous ZnO NFs under different calcination temperatures. Comparing Figure 7a with Figure 7b, the diameter of the fibers is reduced by 80% after calcination at 650 °C, and

the crystallinity and crystal size of the porous ZnO NFs are significantly increased after calcination at high temperatures. The band gap decreases as the crystal size increases, as depicted in Figure 7c. Singh et al. also found that porous ZnO NFs showed good photocatalytic degradation performance for naphthalene and anthracene.

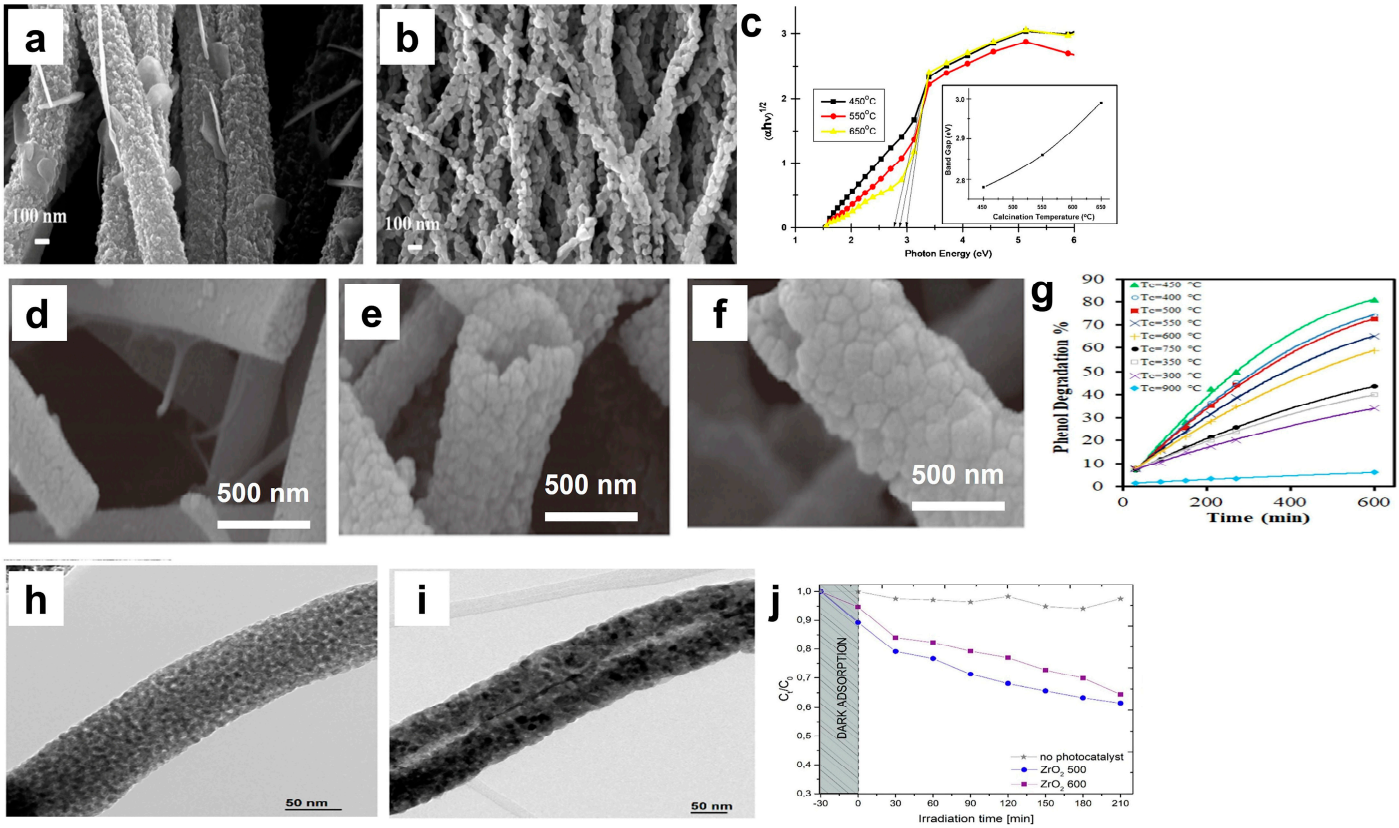

Figure 7. SEM images of ZnO NFs treated at 450 °C (**a**), 650 °C (**b**); the band gap of ZnO NFs treated at different calcination temperatures (**c**) [94], Copyright 2013, Elsevier. SEM images of 5% Ag/TiO_2 photocatalytic NFs treated at 450 (**d**), 600 (**e**), and 750 °C (**f**); the photocatalytic degradation of 5% Ag/TiO_2 treated at different calcination temperatures (**g**) [95], Copyright 2022, Elsevier. TEM images of ZrO_2 500 (**h**) and ZrO_2 600 (**i**) nanostructure; the photocatalytic degradation of ZrO_2 at 500 and 600 °C (**j**) [96], Copyright 2023, Elsevier.

Ag/TiO_2 photocatalytic NFs were prepared [95], and the effects of silver content (0.5–15%) and calcination temperature (300–900 °C) on the degradation of phenol were studied. It can be seen from Figure 7d,f that some cracks appeared on the surface of NFs after being treated under high temperatures. With increase in calcination temperature, the fiber diameter decreased from 5 µm to 500 nm, the boundaries of the grains on the surface of the NFs became clearer, and the grains became rougher. The grains shrunk and the boundaries of the grain appeared to crack with increasing calcination temperatures. This may have been due to the continuous decrease in PVP, or the growth and change in the crystal structure of TiO_2 during the calcination process. This study also found that the highest degradation rate of phenol was 82.65% when the calcination temperature was 450 °C.

Zaborowska et al. [96] prepared $PVP/EtOH/ZrOCl_2/DMF$ one–dimensional zirconia NFs using a uniaxial electrospinning technique. The $PVP/ZrOCl_2$ composite fiber exhibited a smooth and uniform surface, the average diameter being 324 nm. The average diameters of ZrO_2 (500 °C) and ZrO_2 (600 °C) were 162 and 95 nm, respectively. XRD analysis confirmed the existence of monoclinic and tetragonal phases in ZrO_2 (500 °C) and ZrO_2 (600 °C). The specific surface area of $PVP/ZrOCl_2$ composite fiber mats calcinated at 500 °C was 53.8 m^2/g, which was 15 m^2/g higher than the mats calcinated at 600 °C. The bandgap widths of $PVP/ZrOCl_2$ composite fiber obtained at 500 °C and 600 °C were 4.9 and 5.6 eV,

respectively. The larger specific surface area and lower band gap of ZrO_2 NFs treated at lower temperatures contributed to enhancing the photocatalytic degradation performance. Compared with the mats calcinated at 600 °C, the efficiency of MB degradation was only increased by 3%. The photocatalytic degradation performance of fiber mats was not improved significantly by increasing the calcination temperature, so selecting a suitable temperature is very important for improving photocatalytic performance and making rational use of energy.

3.2.2. Carbonization

Carbonization is defined as the heating of materials at high temperatures in nitrogen or other inert gases. By combining electrospinning and carbonization techniques, Song et al. prepared C/TiO_2 NFs [97]. The impact of the carbonization temperature on the electrochemical performance and photocatalytic degradation of MB was investigated. C/TiO_2 NFs prepared at carbonization temperatures at 400, 600, and 900 °C are shown in Figure 8a–c. The diameters of NFs carbonized at various temperatures were uniformly distributed between 280 and 480 nm. The NFs formed network structures and they were continuous and random. The morphologies of the NFs were not appreciably altered by heat treatment. These findings indicated that C/TiO_2 NFs carbonized at 900 °C exhibited the highest capacitance, while C/TiO_2 NFs carbonized at 400 °C had the best photocatalytic activity. The transfer of photogenerated electrons from the conduction band of TiO_2 to carbon was able to improve the separation efficiency of electrons and holes during the photocatalytic process, so the photocatalytic degradation efficiency of C/TiO_2 NFs was increased. This research serves as a guide to the potential for using C/TiO_2 NFs in energy storage technologies and photocatalytic materials in the future.

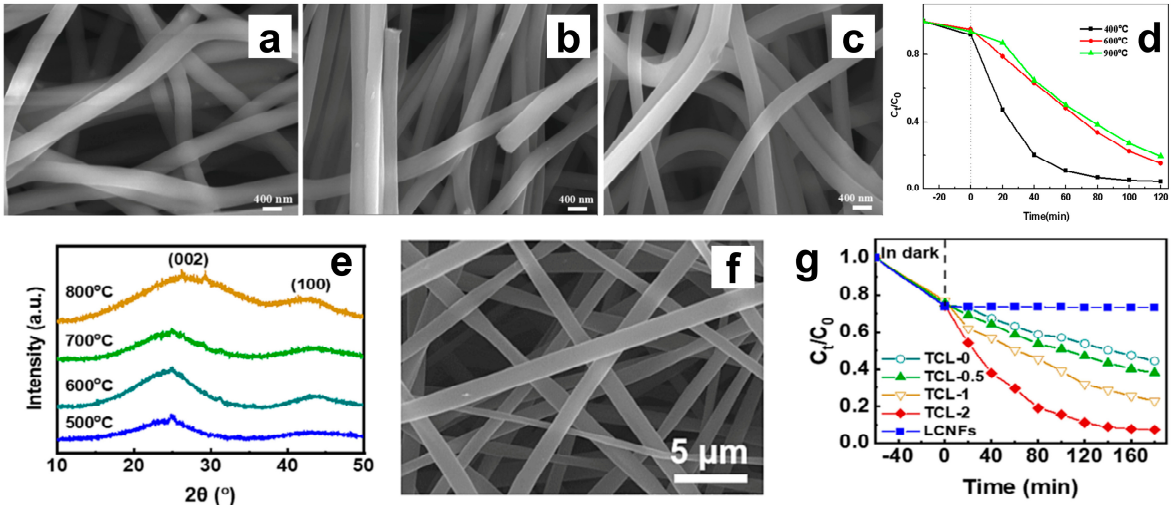

Figure 8. SEM images of C/TiO_2 NFs carbonized at 400 °C (**a**), 600 °C (**b**), and 900 °C (**c**); the photocatalytic degradation of C/TiO_2 NFs (**d**) [97], Copyright 2020, Elsevier. XRD patterns of LCNFs carbonized at different temperatures (**e**), SEM image of LCNFs obtained at 800 °C (**f**); the photocatalytic degradation of TCL to rhodamine B (RhB) (**g**) [98], Copyright 2023, Elsevier.

Zhai et al. [98] loaded TiO_2 and g–C_3N_4 into lignin–based carbon NFs (LCNFs) and then prepared TiO_2/g–C_3N_4@LCNFs (TCL) through carbonization treatment. The spinnability of lignin solutions, the chemical structure and morphology of LCNFs, TiO_2/g–C_3N_4@LCNFs, and the catalytic degradation performance of RhB were studied. Lignin–based precursor NFs were able to be completely carbonized, and melamine was converted into g–C_3N_4 at 600 °C (Figure 8e); the SEM image of it is shown in Figure 8f. Under visible light irradiation, the degradation rate of RhB over TiO_2/g–C_3N_4@LCNFs was 92.76% (Figure 8g). The high photodegradation performance of TiO_2/g–C_3N_4@LCNFs can be attributed to the synergistic effect of TiO_2 and g–C_3N_4; the synergistic effect can improve

the separation efficiency of electrons and holes. This work opens a new direction for the development of high–efficiency photocatalysts based on biomass–derived fiber materials.

3.2.3. Hydrothermal and Solvothermal Technology

Hydrothermal technology refers to the chemical reactions carried out in water at a certain temperature and pressure. Using hydrothermal technology to prepare materials can enrich the structure and functional groups, increase the specific surface area, and improve the performance of materials. Mesoporous TiO_2/In_2O_3 NF was synthesized by electrospinning and hydrothermal technology [99]. In_2O_3 tightly adheres to the surface of TiO_2 NFs, and TiO_2/In_2O_3 hybrid NFs are mesoporous, as shown in Figure 9(a1–a3). This study also found that the additional amount of In_2O_3 plays an important role in the formation of mesoporous NFs. When the raw material weight of In_2O_3 was 53.25 mg (TI–A, Figure 9(a1)), 95.5 mg (TI–B, Figure 9(a2)), and 190.1 mg (TI–D, Figure 9(a3)), the NFs were mesoporous. Compared with TiO_2 and In_2O_3, the mesoporous TiO_2/In_2O_3 NFs exhibited better photocatalytic degradation ability for RhB degradation, as shown in Figure 9b. The improvement in photocatalytic ability can be mainly attributed to more active sites provided by the mesoporous structures, and the expansion of the light response range provided by type II heterostructures. This work provides a new strategy for efficiently constructing mesoporous heterostructure photocatalysts.

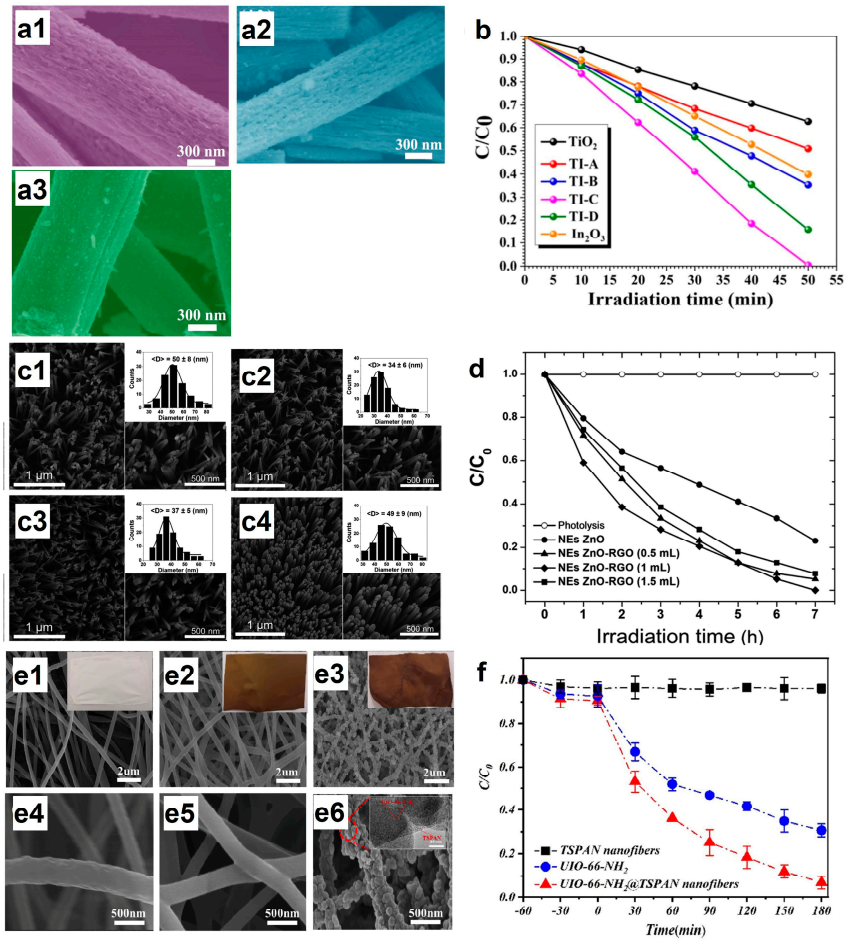

Figure 9. SEM images of TI–A (**a1**), TI–B (**a2**), and TI–D (**a3**), photocatalytic RhB degradation profiles (**b**) [99], Copyright 2021, Elsevier. SEM images of ZnO–RGO seed layers with different amounts of RGO: 0 mL (**c1**), 0.5 mL (**c2**), 1.0 mL (**c3**), and 1.5 mL (**c4**) in the spinning solutions; the photocatalytic degradation of methyl orange (MO) over ZnO–RGO NRs (**d**) [100], Copyright 2019, Elsevier. SEM images of electrospun PAN NFs (**e1**,**e4**), TSPAN NFs (**e2**,**e5**), and UIO–66–NH_2@TSPAN NFs (**e3**,**e6**); the photocatalytic degradation of Cr(VI) over different NFs (**f**) [101], Copyright 2022, Elsevier.

ZnO and reduced graphene oxide (ZnO–RGO) nanorods were grown on tin fluoride oxide (FTO) glass substrates by electrospinning and hydrothermal techniques [100]. Electrospun NFs containing PVP, zinc acetate, and different amounts of RGO were calcinated at 400 °C for 1 h to prepare a ZnO–RGO precursor layer. Then the precursor layer was used for hydrothermal growth of (ZnO–RGO) nanorods. Figure 9(c1–c4) shows that ZnO grew on the surface of the RGO sheets (the areas surrounded by discontinuous white lines). This may have been due to the fact that there was a strong interaction between ZnO NPs and RGO sheets and that the functional groups on the surface of the modified graphene provided sites for aggregation and nucleation of the host material. The average diameter of ZnO NPs which formed ZnO–RGO nanorods decreased as the amount of RGO increased. This was related to the increment in electrical conductivity of the electrospinning solution by the addition of RGO. ZnO–RGO nanostructures containing 1.0 mL of RGO exhibited the highest photocatalytic activity for the degradation of MO, as depicted in Figure 9d.

Solvothermal technology is a synthesis technology based on hydrothermal technology, which refers to mixtures reacted in a closed system using organic or non–aqueous solvents. It differs from hydrothermal reactions in terms of the solvent. Hydrothermal technology is often only applicable to the preparation and treatment of oxide materials or water–insensitive materials. Compounds such as carbides, fluorides, and novel phosphate materials are not applicable for preparation by hydrothermal technologies, so the development of solvothermal technology has been promoted.

A metal–organic framework (MOF) [1] as a precursor for the synthesis of NF membranes has gained prominence. MOF–based NF membranes have the advantages of a distinctive crossing network connection, an extraordinarily wide surface area, and a porous structure. In the synthesis process of MOFs, solvothermal technologies are generally used because the metal ions in MOF are more sensitive to water. Zhou et al. [101] have successfully grown UIO–66–NH_2 on thermally stabilized electrospun PAN NFs (TSPAN) using solvothermal technologies (UIO–66–NH_2@TSPAN NFs) to reduce Cr(VI). TSPAN has high stability and abundant nucleation sites, providing active sites for the growth of an MOF. Figure 9(e1,e4) shows SEM images of electrospun PAN NFs before and after thermal oxidation stabilization treatment. It can be observed that the prepared PAN NFs were randomly distributed, with uniform fiber diameter distribution and a smooth surface. The thermally stabilized TSPAN NFs were cross–linked and had a smoother surface, as shown in Figure 9(e2,e5). The SEM images after the growth of UIO–66–NH_2 are shown in Figure 9(e3,e6). It can be seen that the particles were uniformly distributed on the surface of the NF. The spherical UIO–66–NH_2 particles directly nucleated and grew on the TSPAN NFs, illustrating that UIO–66–NH_2 and TSPAN bound tightly. This is because there are acridone rings, naphthyridine rings, and hydrogen–naphthyridine rings in TSPAN NFs, which can act as reaction sites to promote the heterogeneous nucleation of UIO–66–NH_2. Compared to powdered UIO–66–NH_2, the photocatalytic reduction efficiency of Cr(VI) on UIO–66NH_2@TSPAN was improved by 23% (Figure 9f).

4. The Application of Photocatalytic Degradation of Pollutants in Wastewater

4.1. Photocatalytic Degradation of Dyes

For many industries, including textile, dyeing, papermaking, pulp, tanning and paint, synthetic dyes are essential. Dyes have high water solubility, which makes them challenging to remove and treat. Typically, only 80% of the dye is absorbed by the fabric; the other 20% is desorbed and discharged into the water. Dyes block light from penetrating the water, so that photosynthesis is slowed down and dissolved oxygen levels are reduced, which has an impact on the entire aquatic ecosystem [102]. Furthermore, dyes are poisonous and carcinogenic compounds can enter the entire food chain [103]. It is necessary to remove dyes from wastewater using modern technology. Photocatalysis technology is regarded as an excellent "green strategy" because of its low energy consumption and other environmental advantages. Photocatalysts can produce oxidation species such as $\bullet O_2^-$ and •OH to degrade pollutants such as dyes in wastewater [104]. The widespread

use of photocatalysts is due to their beneficial traits, such as their quick and thorough decomposition of a variety of organic compounds prevalent in water and wastewater, without generation of persistent by–products, and their ease of scaling up.

The earliest electrospinning NFs photocatalysts to degrade dyes were prepared by uniaxial electrospinning technology [23]. The uniaxial NFs prepared by uniaxial electrospinning technology were the origin of complex structural NFs. As the simplest NF with the simplest structure, uniaxial NFs have the advantages of easy preparation, simple operation, and capacity to load a variety of functional materials. The membrane materials prepared by this technology are widely used for the photocatalytic degradation of pollutants in water [1,38]. In order to improve the photocatalytic performance, Zhou et al. [105] consistently integrated g–C_3N_4 onto bacterial cellulose (BC) with a 3D NF network. In contrast to the modification of polypyrrole (PPy) in most research, developing carrier materials and reactors can significantly increase the catalytic performance. The prepared PPy@(BC/g–C_3N_4) flexible membrane was used under a xenon lamp ($\lambda > 420$ nm) in the designed reactor. It exhibited strong catalytic performance (64.28%, 2 h), which was 5.27 times higher than BC/g–C_3N_4. After 10 cycles, more than 80% of the original catalytic performance was sustained. This research can be also applied to design flexible membrane materials with excellent photocatalytic performance [20]. A positive feature of this study was the loading of the functional materials layer–by–layer onto the BC. In this study, the BC mainly acted as a load carrier. The g–C_3N_4 was responsible for visible light absorption and photocatalytic degradation for the entire material. The primary function of PPy is conductivity because the essence of photocatalysis degradation is the transfer of e^- and h^+. PPy can guide e^- in time to achieve the purpose of e^- and h^+ separation. However, the e^- and h^+ can still be readily combined. How to solve the combination of e^- and h^+ in the same type of particle is a problem that future research should address.

With the development of electrospinning technology, coaxial electrospinning technology has also emerged, in which the photocatalytic degradation performance of NF membranes prepared using coaxial electrospinning is improved. Coaxial electrospinning technology has two independent parts. By controlling the flow rate of the injection pump, the thickness of the shell layer of the NF can be adjusted, and even NF membranes with hollow structures can be prepared. The mechanical and photocatalytic performance of the NF membrane can be controlled by varying the thickness of the shell layer [106]. Compared with uniaxial NF membranes, NF membranes prepared using coaxial electrospinning technology have greatly improved mechanical properties [38]. Limiting the functional particles in the shell area can save a portion of the functional particles. In addition, using appropriate solvents can expose functional particles to the surface of NF, which can improve photocatalytic performance.

Coaxial electrospinning was used to prepare a new structure with TiO_2 micro–/nano–spheres embedded in NFs [106], as illustrated in Figure 10a. The construction technology of the structure and the impacts of the core flow rates on photocatalytic capabilities were explored. Moreover, their photocatalytic performances were compared to those of comparison samples. The TiO_2 micro–/nano–spheres were embedded in the NFs with various core and shell–spinning solutions and physical characteristics. The degradation efficiency for MB was 91.56% when the specific surface area of the NFs was 23.852 m^2/g. There were substantial NF gaps in the innovative construction. The micro–/nano–spheres had a large specific surface area and loose structure and were amenable to UV injection to boost the photocatalytic efficiency. In this study, the TiO_2 micro–/nano–spheres were firmly fixed in the NF membrane by the coaxial electrospinning technology, which was able to reduce the loss of functional particles in the repeated cycle experiment and contribute to the maintenance of photocatalytic performance. However, the mechanical properties of the membrane may have been greatly weakened after calcination, and there were many functional particles embedded in the membrane. Suitable experimental design is important to improve the photocatalytic performance in the second cycle process, and the mechanical properties of membranes.

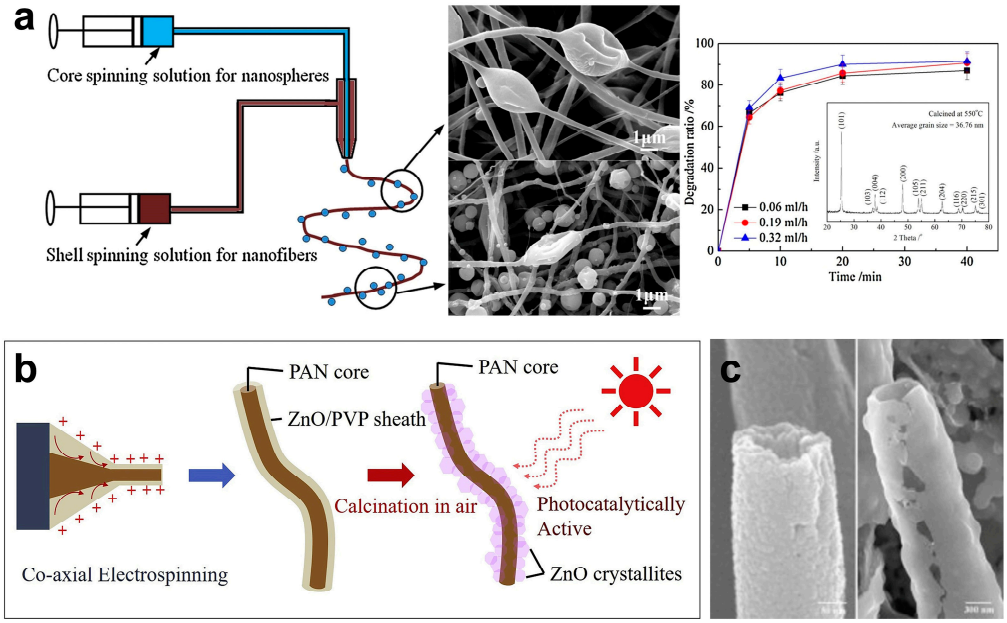

Figure 10. Schematic diagram of preparing hollow TiO_2 NFs and SEM image of TiO_2 micro–/nano–spheres embedded in NFs and degradation rate of MB (**a**) [106], Copyright 2016, Elsevier. Schematic diagram of preparing ZnO/PVP coaxial NFs (**b**) [107], Copyright 2020, Elsevier. SEM image of hollow TiO_2 NFs (**c**) [108], Copyright 2013, Elsevier.

Large surface areas, prevention of nanoparticle aggregation, and easy separation from wastewater are all provided by NF membrane photocatalysts. In one study, flexible PAN was coated with ZnO photocatalysts in a single–step using sol–gel coaxial electrospinning [107], as shown in Figure 10b. In order to remove the PVP and crystallize the ZnO, a core/sheath structure made of a PAN polymer embedded in a ZnO–PVP mixture was prepared. To identify the ideal parameters for preparing NFs, the PAN and PVP concentrations and viscosities were changed. Thermogravimetric analysis and Fourier transform infrared spectroscopy were used to evaluate the thermal behavior and ideal calcination temperature. The flexibility and photocatalytic activity for the degradation of the MB of the NFs were maintained after several cycles. In this study, ZnO was mainly responsible for photocatalytic degradation. However, ZnO can only absorb ultraviolet light, which seriously limits its practical application. The mechanical properties of NF membranes are improved with the use of coaxial electrospinning technology. However, NF membranes calcinated in air are fragile, which is not conducive to later recovery and treatment.

A simple coaxial electrospinning approach was used to design two kinds of hollow TiO_2 NFs [108]. Titanium sol and a titanium precursor were used for the shell of two kinds of hollow TiO_2 NFs. The two types of hollow TiO_2 NFs shared a similar tubular structure on the nanoscale, although they differed in size and shell thickness. An SEM image of hollow TiO_2 NFs is depicted in Figure 10c. Hollow NFs made from titanium sol showed that the diffusion of the core and shell solutions may have been effectively prevented by a modest amount of water in the core. In order to develop the titanium precursor into the nanostructured TiO_2 wall of the hollow NFs, it was coated on the PVP core NFs as a shell template by coaxial electrospinning. The hollow TiO_2 NFs showed greater photocatalytic activity for the degradation of MB than uniaxial TiO_2 NFs. In this study, TiO_2 hollow NFs were obtained by coaxial electrospinning and high–temperature calcination. The hollow NFs had a large specific surface area and more active sites for photodegradation. Compared with uniaxial NFs, the photocatalytic performance was improved. However, the high–temperature calcination treatment seriously limits its mechanical properties, which makes it difficult to apply in practical environments in the future.

Peng et al. [109] prepared highly uniform SnO_2/TiO_2 coaxial NFs with an adjustable interior morphology by one–pot step coaxial electrospinning. The core of these NFs was able to be varied from filled solid to peapod–like, and even to hollow tubes, by changing the concentration of the precursor solution. The degradation rate of RhB was 4.6×10^{-3} cm^{-1} (Tubular SnO_2/TiO_2 coaxial NFs). It was discovered that the photocatalytic activity of commercial TiO_2 photocatalysts was lower than that of tubular SnO_2/TiO_2 coaxial NFs. This finding was explained by the formation of a heterojunction between SnO_2 and TiO_2; the coaxial structure also an important role. The overall findings suggest that coaxial electrospinning can be used as a unique, simple technology for designing one–dimensional inorganic coaxial nanoscale heterostructures on a large scale. It can also be used for a variety of other purposes. This study ingeniously used oil to prepare coaxial NFs, which provides a direction for the preparation of such NF membranes in the future. However, the oil used in this study has certain limitations. The materials mixed with oil can easily come out of the membrane during catalytic treatment, which can cause secondary pollution to the water. The compatibility of the oil and the outer material in the electrospinning process should also be solved. In addition, looking for other materials to prepare coaxial nanostructures to enhance photocatalytic performance is important.

Janus NF membranes have been prepared by side–by–side electrospinning technology [57]. This technology is similar to coaxial electrospinning technology. Both have two independent parts. The difference between them is that the form of side–by–side electrospinning technology is similar to the p–orbit electronic cloud, with the two parts only having a small amount of contact. The contact point can form a heterojunction. The combination rate efficiency of e^- and h^+ is greatly depressed and the efficiency of photocatalytic degradation is improved. Side–by–side electrospinning technology can reduce the inappropriate agglomeration between different kinds of particles. The structure of the design material can achieve an ideal photocatalytic effect, which provides a good example for the future photocatalytic treatment of pollutants in water.

(ZnO/PAN/DMF)//($Mn_3O_4CeO_2$/PAN/DMF) Janus NFs were electrospun in [110]. The Janus NFs consisted of ZnO NF on one side and Mn_3O_4/CeO_2 NF on the other. Using the MB solution, the photocatalytic performance was verified. The as–prepared Janus NFs outperformed conventional NFs (CFs) in terms of photocatalytic performance under UV and visible light. The results also showed that it was feasible to alter their photocatalytic activity under the appropriate light wavelength by varying the ratio of photocatalyst weights on each side of the Janus NF. Water purification, photocatalysis, and other applications can greatly benefit from membranes made of functional Janus NFs prepared using a specifically designed nozzle. ZnO, Mn_3O_4, and CeO_2 were used to realize the absorption of materials in different light bands. The Janus heterojunction was formed using an ingenious electrospinning design. Uniaxial and coaxial NFs membrane have the problem of e^- and h^+ combination, this kind of Janus NFs can solve this problem because different kinds of particles are separated in different parts. However, compared with coaxial NF membranes, the material also has certain defects in mechanical properties.

Through conjugate electrospinning and the subsequent calcination procedure, a [TiO_2/C]/[Bi_2WO_6/C] Janus NF heterojunction photocatalyst (JNHP) was conceived and built [20]. The JNHP with a distinctive Janus structure has two aspects: TiO_2/C NF responds to ultraviolet light, and Bi_2WO_6/C NF responds to visible light, as shown in Figure 11a. JNHP exhibited excellent MB degradation. Under visible light and sunlight irradiation, the MB degradation efficiencies of JNHP were 93.3% (160 min) and 97.9% (140 min), respectively. Compared to TiO_2/C and Bi_2WO_6/C photocatalysts, the photocatalytic activity of JNHP was improved, which primarily resulted from the cooperative effect of novel heterojunctions between TiO_2 and Bi_2WO_6, and conductive carbon NF. Additionally, JNHP showed great recyclable stability. The Bi_2WO_6 nanoparticle (NP) can absorb light to create e^-–h^+ pairs and excite the e^- from the Bi_2WO_6 (VB) to the conductive band (CB) when the surface of the JNHP is exposed to visible light. The e^- on CB can easily move to the CNF because of the excellent conductivity of CNF. Additionally, it is simple

to transfer the h^+ on the VB of Bi_2WO_6 to the VB of TiO_2. The e^- and h^+ are successfully separated and involved in the oxidation reaction because TiO_2 and Bi_2WO_6 can form a heterojunction. The h^+ on the VB of JNHP quickly moves to the surface of JNHP, and h^+ is oxidized with the MB molecule during the photodegradation process of MB. At the same time, O_2 can absorb e^- by dissolving in water to produce $\bullet O_2^-$, which combines with H_2O to form •OH. The active oxidation properties of chemicals •OH and $\bullet O_2^-$ can destroy MB molecules, as shown in Figure 11b,c. The Janus NF membrane preparation technology in this study is novel, and the proposed Janus NF heterojunction is innovative. In addition, the treatment of NF membranes in N_2 solves the problem of material fragility, which provides an example for the preparation of self–supporting Janus NF heterojunction materials in the future. However, due to the defects of PAN and conjugated electrospinning technology, the material has the disadvantage of a low parallel rate in the preparation process, which leads to the preparation of too few Janus NFs. How to solve this problem is particularly important.

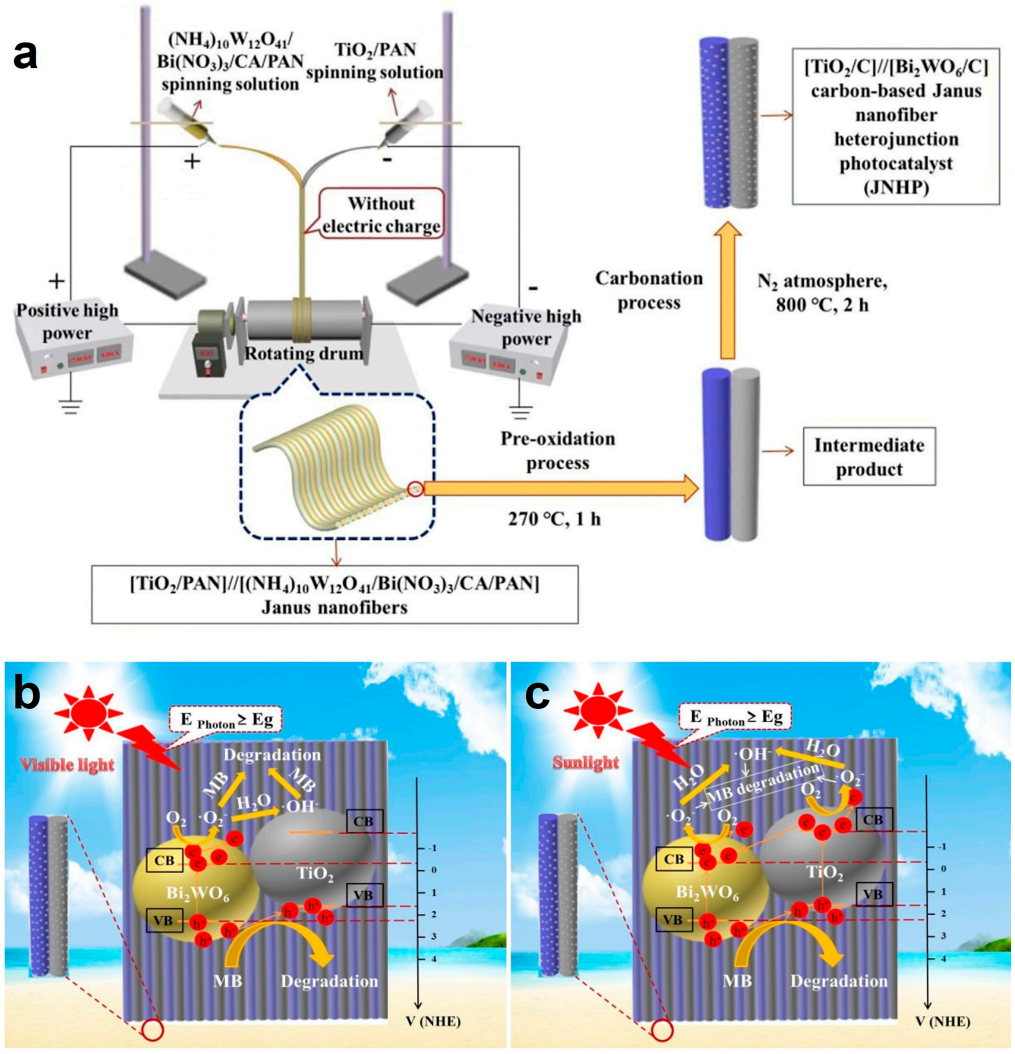

Figure 11. Schematic illustration of the preparation procedure of JNHP (**a**) and photocatalytic degradation mechanism (**b**,**c**) [20]. Copyright 2020, Elsevier.

The photocatalytic degradation performance of NF membranes prepared by different electrospinning techniques are shown in Table 1. These membranes show extensive application abilities in the degradation of MB. By comparison, it can be seen that Janus NF membranes have the highest degradation efficiency and the lowest energy consumption, which is related to the special structure of NFs prepared by improved electrospinning

technology. The formed special structure of NFs can improve the separation efficiency of electrons and holes, so the photocatalytic performance can be improved. However, the low mechanical properties, permeability, and high energy consumption of electrospun NF membranes need to be further resolved.

Table 1. Photocatalytic degradation performance of NF membranes prepared by different electrospinning techniques.

Photocatalytic Electrospinning Membrane	Technology	Pollutants	Source Light	Photocatalytic Degradation (%)	Degradation Time (min)	References
TiO_2/g–C_3N_4 fibers	Uniaxial electrospinning	MB	Xenon lamp (200 nm cutoff)	90%	20 min	[9]
TiO_2 micro–/nano–spheres coaxial NFs	Coaxial electrospinning	MB	UV light 365 nm	91.56%	40 min	[106]
ZnO/PAN/PVP NF	Coaxial electrospinning	MB	UV lamp 15 W	80%	6 h	[107]
TiO_2 hollow NFs	Coaxial electrospinning	MB	mercury lamp (200 W, λ_{max} = 365 nm	99%	50 min	[108]
(ZnO/PAN/DMF)//($Mn_3O_4CeO_2$/PAN/DMF) Janus NF	Parallel electrospinning	MB	MR16 lamp (50 W)	100%	2 h	[110]
[TiO_2/C]/[Bi_2WO_6/C] Janus NF	Conjugate electrospinning	MB	Xenon lamp (400 nm cutoff)	100%	140 min	[20]

4.2. Photocatalytic Degradation of Antibiotics

Antibiotics are employed as growth boosters in animal husbandry or to prevent and treat infectious infections in humans, animals, and plants [111]. The majority of antibiotics, along with urine and feces, are expelled into the environment as compounds, and they cannot be completely absorbed by the body [112]. Moreover, the majority of antibiotics are soluble in water, so it is easy to mix them with water in the environment. Antimicrobial pollutants have a considerable impact on antibiotic–resistant bacteria and genes, which can readily encourage the formation of "super bacteria" and constitute a serious threat to human health and environmental stability [113], so the antibiotics must be treated immediately. The photocatalytic degradation technique is outstanding because it can break down antibiotics into non–toxic compounds, water, and carbon dioxide; it is safer and more efficient than other methods.

Electrospinning was used to prepare SiW_{12}/CA composite NF membranes. SiW_{12} has successfully coupled with CA [114]. According to FT–IR, EDS, and XPS measurements, the Keggin structure of the composite membrane was unchanged. Due to the high porosity and specific surface area of the NF membrane, electrospun CA NFs offer additional contact regions and reaction sites between SiW_{12} and tetracycline (TC) during the photodegradation. As a result, the SiW_{12}/CA composite NF membrane has higher photocatalytic activity than SiW_{12} NPs. In addition, CA additionally supplies electrons to SiW_{12} leading to higher degradation efficiency. It can be concluded that CA membranes play various roles in the photodegradation of MO and TC, which involve various photocatalytic pathways and various degradation rates, as shown in Figure 12a. Most importantly, the composite membrane is ideally suited to practical applications and has exceptional reusability. As a result, SiW_{12}/CA NF membranes can be extensively employed to remove organic contaminants.

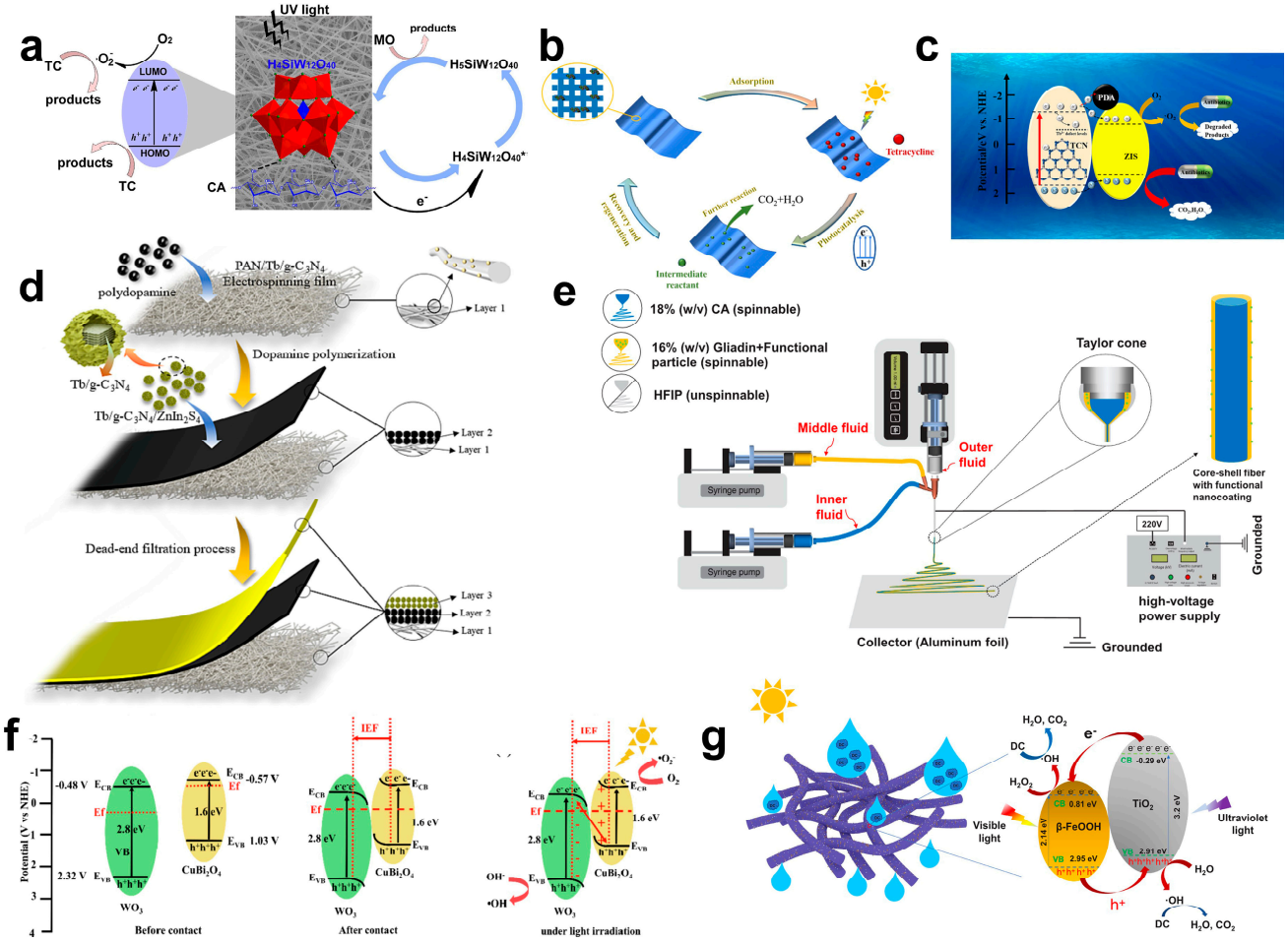

Figure 12. Photocatalytic mechanism diagram of SiW_{12}/CA nanofibrous membrane for degradation of TC and MO (**a**) [114], Copyright 2017, Elsevier. Adsorption and photocatalytic regeneration diagram of PAN/BT fiber membrane (**b**) [115], Copyright 2022, Elsevier. Diagram of the photocatalytic mechanism of PPTZ (**c**), the synthetic route of PPTZ (**d**) [116], Copyright 2023, Elsevier. Energy level diagram of $CuBi_2O_4$@WO_3 before and after contact; S–scheme charge transfer diagram (**f**) [117], Copyright 2023, Elsevier. Schematic diagram of improved triaxial electrospinning technologies and photocatalytic mechanism of β–FeOOH/TiO_2 membrane (**e**,**g**) [16], Copyright 2021, Elsevier.

Electrospinning was used to prepare a PAN/Bi_2MoO_6/Ti_3C_2 (PAN/BT) NF membrane [115]. It demonstrated high photocatalytic activity and was able to break down 90.3% of TC under visible light. In Figure 10b, the routes for treating TC are depicted. TC in water is adsorbed by using functional groups on the surface of the membrane. The Bi_2MoO_6/Ti_3C_2 heterojunction in the membrane may efficiently degrade TC in the photocatalytic degradation stage. At the same time, the PAN/BT NF membrane showed a consistent recovery performance, and the degradation efficiency was maintained at 80% after three recoveries. According to this research, the built Bi_2MoO_6/Ti_3C_2 heterojunction can significantly enhance photocatalytic performance. The regeneration capabilities of the electrospun fiber membranes provide a new avenue for investigating the affordable and effective degradation of antibiotics in water.

Membranes are employed as carriers and bulk photocatalysts can be deposited in them. The restriction of low powder recovery can be reduced and recovery performance can be enhanced. The reuse rate and recovery efficiency of photocatalysis powder can also be increased. Wang et al. [116] used electrospinning and coating techniques to create a three–dimensional layered photocatalytic fiber membrane. Figure 12d illustrates the PAN, polydopamine (PDA), and Tb–doped graphitized carbon nitride/$ZnIn_2S_4$

(Tb–g–C_3N_4/$ZnIn_2S_4$) (PPTZ) membrane. Under simulated sunlight, the photocatalytic performance of the prepared composite membrane was investigated. Compared with PAN@Tb–g–C_3N_4 (PT) and PAN@PDA/Tb–g–C_3N_4 (PPT), the photocatalytic efficiency of PAN@PDA/Tb–g–C_3N_4/$ZnIn_2S_4$ (PPTZ) was highest. Tylosin (TYL) and TC were degraded by PPTZ, the degradation rates being 2.1 and 2.5 times higher than those of the other samples, respectively. As illustrated in Figure 12c, electrons can be transferred using PDA as the medium from Tb–g–C_3N_4 to $ZnIn_2S_4$. The construction of heterostructures between Tb–g–C_3N_4, $ZnIn_2S_4$, and PDA can boost the separation efficiency of photogenerated carriers, so the photocatalytic activity of PPTZ is outstanding. In addition, the toxicity of the membrane has been studied, and the membrane would not cause secondary pollution in practical applications.

Zhang et al. [117] prepared photoresponsive–optical $CuBi_2O_4$@WO_3 fibers by combining electrospinning technology with post–calcination technology. It has an S–type heterojunction structure, as shown in Figure 12f. The degradation efficiency of TC on $CuBi_2O_4$@WO_3 was 70.42% within 2 h, much higher than for pure $CuBi_2O_4$ (30.42%) or pure WO_3 (15.89%). There are three reasons for the increment in photocatalytic activity: 1. An interface of charge transfer and separation is formed between WO_3 NFs and $CuBi_2O_4$ NPs; 2. NFs and NPs provide a large number of reactive sites for photocatalytic reactions; 3. The S–heterojunction in $CuBi_2O_4$@WO_3 provides sufficient holes and electrons for WO_3 and $CuBi_2O_4$ and provides the prerequisite for the separation of carriers in photocatalytic reactions. This work provides a new way to construct new types of heterostructures to treat antibiotics under visible light irradiation by electrospinning technology.

The NFs prepared from uniaxial and coaxial NFs have functional limitations, such as: 1. Mixing of different kinds of particles may accelerate the recombination of photogenerated carriers; 2. The photocatalytic degradation efficiency cannot meet the demand by adding a single kind of material; 3. If too many functional particles are added, it will be difficult to electrospin during the electrospinning process. Therefore, multi–level electrospinning has emerged. Using heating, calcination, and improved triaxial electrospinning technologies (Figure 12e), Zhao et al. [16] prepared a variety of NPs and NF membranes; doxycycline (DC) was chosen as a pollutant. Under sunlight, the functional NF membrane loaded with β–FeOOH/TiO_2 (1/1, *w*/*w*) exhibited the best DC degradation. The ideal concentration of H_2O_2 was 9 mmol/L, while the ideal pH for degradation was 6. The maximal natural photodegradation efficiency for DC was 90.14% in 5 h. Two semiconductor materials (β–FeOOH and TiO_2) were responsible for the enhancement of photocatalytic degradation, and their suitable band potentials played key roles in the higher photo–induced carrier separation efficiency. Moreover, electrospun NF membranes can be used as carriers to create multifunctional electrospun membranes, which have enormous potential for use in real–world pollutant photodegradation.

4.3. Photocatalytic Degradation of Heavy Metal Ions

With the expansion of sectors such as electronic manufacturing, electroplating, chemical processing, mechanical manufacturing, and oil refining, heavy metals have become more and more necessary [118]. Through sewage discharge, rainfall corrosion, air deposition, and other pathways, various kinds of heavy metals enter the water. Exposure to significant quantities of heavy metals, which are highly hazardous and carcinogenic compounds, can kill organisms [119]. Heavy metal ions in water cannot be entirely treated using conventional membrane separation, electrolysis, and adsorption technologies. Heavy metal ions can be converted to non–toxic materials by photocatalytic technology, which increases the efficiency and safety when treating heavy metal ions [120].

UiO–66–NH_2 was doped into 4,4,4,4–(porphyrin–5,10,15,20 tetrayl) tetrakis (benzoic acid) (TCPP) ligand (Zr–TCPP) by one–pot electrospinning technology, and was then coordinated with different amounts of Ag^+ using –NH_2 [121]. Ag NPs were then in situ encapsulated in Zr–TCPP under ultraviolet light (Ag NPs@Zr–TCPP (ZATx)). The effects of pH, Cr(VI) concentration, and the presence of inorganic salts on the photocatalytic degradation efficiency

for Cr(VI) were also studied. The results showed that ZATx exhibited excellent photocatalytic reduction performance for Cr(VI) under acidic conditions with a Cr(VI) concentration of 100 mg/L in the presence of inorganic salts, because of the light absorption ability of TCPP and the electron transfer ability of Ag NPs in the photocatalytic process. In addition, NF membrane filters were also prepared using electrospinning technology. ZATx/PAN still exhibited an excellent photocatalytic degradation effect for Cr(VI). This research not only expands the application of traditional powder photocatalysts in photocatalysis, but also provides insights into the reconstruction strategy of photocatalysts. It also paves the way for the development of efficient photocatalysts with environmental benefits.

A cellulose–based FeOOH@MIL–100 (Fe)/CeP electrospun NF membrane with core–sheath structure and high photocatalytic activity for simultaneous dye degradation and Cr(VI) reduction was prepared [122]. The β–FeOOH@MIL–100 (Fe)/CeP electrospun NF membrane has ultra–high MIL–100 (Fe) (78 wt%) loading rate and super wettability (WCA = 0° in air). Due to the deacetylation of CA and partial solvent leaching of PVP, the immobilization of hydrophilic MIL–100 (Fe) crystals is promoted, which is conducive to the treatment of complex wastewater systems containing oil–water lotion, organic dyes, and heavy metal ions. B–FeOOH@MIL–100 (Fe)/CeP electrospun NF membranes have the following advantages: (1) The electronegativity of the β–FeOOH surface is conducive to the adsorption of Cr(VI); (2) β –FeOOH@MIL–100 (Fe) heterojunctions improve the absorption and utilization of visible light, and promote the separation of electrons and holes; (3) The combination of iron ions (Fe) in β–FeOOH@MIL–100 and visible light forms a photo–Fenton synergistic effect, which promotes the rapid degradation of pollutants. The heterojunction in the core–sheath structure of FeOOH@MIL–100 (Fe)/CeP electrospun NF membrane can not only be used as an adsorbent for dye, but also acts as a photo–Fenton catalyst. It produces a membrane with high pollutant degradation and self–cleaning capabilities, as well as good cycle stability. The degradation efficiency of Cr(VI) by β –FeOOH@MIL–100 (Fe)/CeP electrospun NF membrane was 99.7%.

4.4. Photocatalytic Degradation of Bacteria

The complex existence of various bacteria and viruses in water poses a significant threat to humans and they have become a global problem [123]. Therefore, developing antibacterial strategies is necessary to prevent infection caused by pathogens. Photocatalysis is a technology for treating different bacteria in water [124]. Active free radicals can oxidize and kill most bacteria and pathogens.

PAN and TiO_2 were electrospun into NFs [125], and antibacterial tests were conducted using *E. coli* and Bacillus. The results showed that the PAN/TiO_2 NF membrane hindered the growth of these bacteria under visible light; the membrane had a greater impact on the Gram–positive bacterium Bacillus. It can be seen from Figure 13(a1,a2) that the PAN/TiO_2 NF membrane has a certain inhibitory effect on the growth of both Gram–positive and negative organisms. There are two reasons for this: 1. Active oxygen generated during the photocatalytic process can kill bacteria; 2. Bacteria that accumulate on the surface of the fiber are eliminated by photocatalysts, especially Gram–positive bacteria. Compared to the control sample (bacteria only), the bacterial density of the PAN–TiO_2 NF membrane decreased slightly under dark conditions. Because the catalytic ions on the PAN/TiO_2 can adsorb bacteria inhibiting bacterial growth.

A Ag_3PO_4/P25 NFs membrane was prepared by electrospinning [87], and then a portion of PVP was removed because PVP is water soluble. P25 NFs had no antibacterial activity in the dark (Figure 13(b2)). Ag_3PO_4/P25 NFs showed significant antibacterial effects because there were no bacterial cells, as shown in Figure 13(b3). Under the light, the Ag_3PO_4/P25 NF membrane can produce more reactive oxygen species (ROS), and the •OH produced by electron–hole pairs can react with cell proteins, membranes, and DNA; finally, the cells will die. In the dark, the oxidized Ag and Ag^+ have bactericidal properties, leading to bacterial inactivation. This work solves the problem of nanoparticle loss in solution and opens a new direction for future research on antibacterial materials.

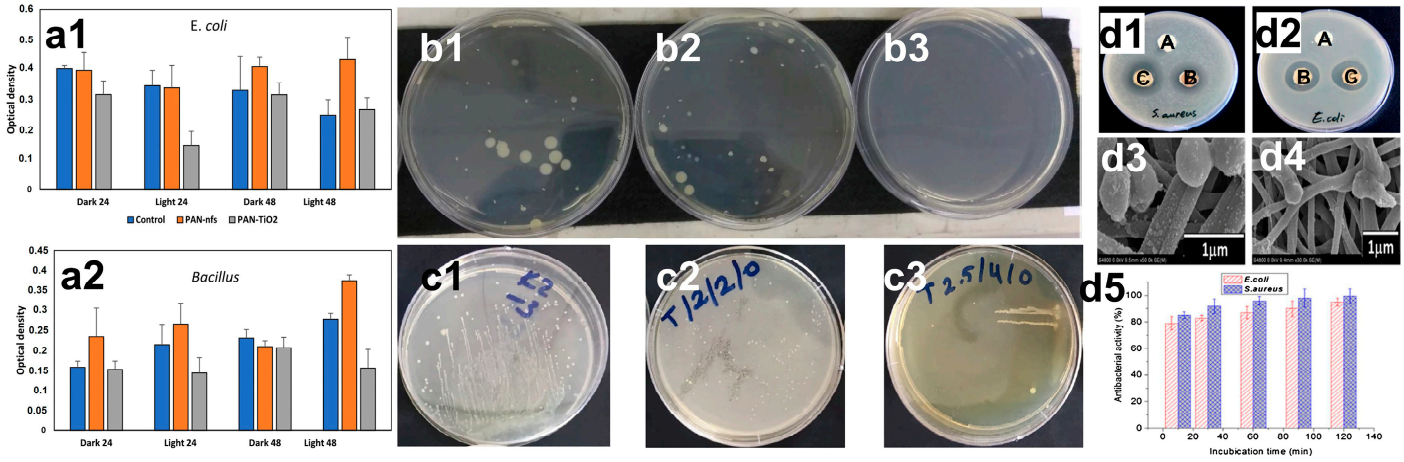

Figure 13. The optical density of *E. coli* (**a1**) and Bacillus (**a2**) under dark and light [125], Copyright 2021, Elsevier. The E.coli colonies without NFs (**b1**), after contact with P25 (**b2**) and Ag_3PO_4/P25 NFs (**b3**) [87]. Colony counts images of *E. coli* contact with pure TiO_2 (**c1**) TiO_2 doped with 2% Ag NPs (**c2**), and TiO_2 doped with 2.5% Ag NPs (**c3**) [126], Copyright 2022, American Chemical Society. The inhibition zone of various NF membranes: PAN membrane (A), PAN/Ag membrane (B), and PAN/Ag/TiO_2 membrane (C) contact with *S. aureus* (**d1**) and *E. coli* (**d2**); SEM images of *S. aureus* (**d3**) and *E. coli* (**d4**) contact with PAN/Ag/TiO_2 NF membranes; the bactericidal activity of PAN/Ag/TiO_2 NF membranes (**d5**) [127], Copyright 2020, Elsevier.

Ag–TiO_2 nanocomposite membranes [126] with different contents of TiO_2 and Ag NPs were successfully prepared by the combination of sol–gel and electrospinning technologies. The *E. coli* cells on the membranes after 24 h of incubation are shown in Figure 13(c1–c3). The doping of Ag NPs significantly improved the inhibition rate against *E. coli*. Compared to other membranes, the TiO_2 nanocomposite membranes doped with 2.5% Ag NPs had higher antibacterial efficiency (99.999%) (Figure 13(c3)). The high bactericidal effect of Ag NP–doped membranes may have been due to the induction of reactive oxygen species (ROS), which were formed by the interaction between silver ions and bacterial cell walls. Ag NPs trigger the formation of free radicals, which can damage bacterial cell membranes. On the other hand, more oxidative stress forms in the cells when the level of ROS increases, leading to cell membrane damage.

Ag/TiO_2/PAN composite NFs [127] were prepared by needleless electrospinning. The addition of $AgNO_3$ significantly increased the electrical conductivity of the spinning solution. In addition, DMF was used as a reducing agent to form Ag NPs in the electrospinning solution. The antibacterial properties of Ag/TiO_2/PAN composite NFs against *E. coli* and *S. aureus* were tested using agar plate technology (Figure 13(d1,d2)). For the pure PAN NF membrane, there were no inhibitory regions against these two bacteria, which is consistent with the non–bactericidal properties of PAN. It is worth noting that inhibition regions were observed for the membranes containing Ag and Ag/TiO_2, and the inhibition regions of Ag/TiO_2 samples were larger than those of the Ag–containing membranes. The results showed that 95% of *E. coli* and 99% of *S. aureus* were killed within 2 h, as shown in Figure 13(d5). The high antibacterial activity was attributed to Ag NPs with large surface areas, which were able to increase the chances of connection between NPs and bacteria to promote antibacterial effects. Moreover, the antibacterial activity of Ag NPs may have been caused by the formation of free radicals and subsequent free radical–induced membrane damage. The irregular shape of pits at the outer membrane of cells was caused by metal depletion. This changed the permeability of the membrane and allowed the release of lipopolysaccharide molecules and membrane proteins. Most importantly, the results suggest that the combination of silver and TiO_2 can achieve excellent antibacterial properties and have synergistic antibacterial effects against *S. aureus* and *E. coli*.

Potential secondary contamination may result from the partial or incomplete degradation of pollutants. Pollutants must undergo complete photodegradation before finishing treatment and entering the water body, so photocatalytic membranes are essential. The photocatalysts carried by the electrospun fiber membrane allow pollutants to adsorb onto its surface before photodegradation and to complete the destruction of organic pollutants. However, if too many photocatalysts are employed, some of them will detach from the reaction. Moreover, using too many photocatalysts can result in photogenerated carriers recombining too quickly. This can decrease the performance of the photocatalytic system, resulting in secondary pollution. Hence, developing photocatalytic NF membranes for the degradation of diverse pollutants in the future will require enhancing the supporting photocatalyst and electrospinning technology.

5. Conclusions and Perspective

NF membranes prepared by electrospinning technology show excellent performance and have important potential applications in the photocatalytic degradation of pollutants in water [101,128–130]. However, the existing electrospinning technology, materials, and industrialization issues limit the photocatalytic efficiency and practical applications [122,131–133]. Multi–fluid electrospinning technology can solve the problem of the low efficiency of electrospinning technology preparation, and further improve the efficiency of the preparation of materials. For example, improvement in tri–axial and parallel electrospinning technology can solve the problem of lower loading function particles and the difficulty of spinning [134–137]. In addition, multi–fluid electrospinning technology can also prepare idealized materials according to actual needs, which is conducive to further practical applications [138–140]. A novel platform can be built to create an increasing number of functional nanostructures for environmental remediation based on the combination of modified coaxial electrospinning and several active substances to address environmental pollutants. The development of novel nanomaterials and associated applications by modified coaxial electrospinning with a non–electrospinnable liquid as the working fluid for the sheath is still in its infancy. Future predictions indicate that there will be an increase in the number of options. With one or more electrospinning fluids, such as tri–axial and parallel electrospinning, non–electrospinning fluids can be processed in a variety of ways. Photocatalysts can be evenly distributed on the surface of polymer NFs using a non–electrospun solution as the sheath working fluid, enhancing photocatalytic performance. Combined with other techniques, modified coaxial electrospinning might further increase its performance.

Finding new photocatalytic particles and improving the photocatalytic efficiency is also a problem that we should face in the future. For example, identifying materials with a lower separation rate of e^- and h^+, oxygen vacancy materials [141,142], carbon materials [143,144], doping composite materials [145,146], triboelectric materials [147,148], piezoelectric materials [149,150], etc., will further improve photocatalytic efficiency. Improving the crystal structure and optimizing the material structure can help to solve the problem of the separation efficiency of e^- and h^+. In addition, the material can make full use of energy existing in nature, such as water energy, wind energy [149,150], friction energy [147,148], etc., to improve treatment efficiency and reduce the emission of greenhouse gases. A hollow structure, confined structure, porous NFs, and porous photocatalysts should be prepared to reduce e^-–h^+ recombination and increase the active sites for the photocatalytic reaction of materials [151,152]. Moreover, the preparation steps of materials should be further simplified to reduce excessive energy consumption. New suggestions and supports can be proposed for developing novel materials to combine electrospinning and advanced oxidation technologies [153–155], such as synthetic strategies, and taking advantage of polymeric special properties as well as filament–forming properties [156,157].

The issue of industrialization needs to be further investigated and developed. For example, how to achieve large–scale production, how to design experiments in actual water bodies to examine the effects of the influence of light–aging and actual conditions on photocatalytic degradation efficiency, and how to improve the mechanical properties of

materials to reduce the problems of practical application, etc. Determining biological toxicity is also an important step in industrial production. Developing environmentally friendly polymers and photocatalytic particles is an important issue for future research. Given the above problems, combining photocatalytic technology with the structural optimization of electrospinning NFs to treat sewage in the future may not only have the advantages of simple and stable structure and easy recycling, but also greatly improve photocatalytic efficiency. Establishing reasonable structural relationships and using materials for high efficiency, fast, and stronger photocatalytic efficiency, is of great significance for the future economy, humanity, and national construction.

Author Contributions: Conceptualization, D.-G.Y. and Y.L. (Yanan Liu); funding acquisition, D.-G.Y.; project administration, D.-G.Y.; writing—original draft, H.L.; writing—review and editing, D.-G.Y., H.L., Y.B., H.S., W.Z., Y.C., Y.L. (Yanan Liu) and Y.L. (Yang Liu). All authors have read and agreed to the published version of the manuscript.

Funding: This work was supported by the Natural Science Foundation of Shanghai (No.20ZR1439000).

Data Availability Statement: The data supporting the findings of this manuscript are available from the corresponding authors upon reasonable request.

Conflicts of Interest: The authors declare no conflict of interest.

References

1. Du, Y.; Yu, D.-G.; Yi, T. Electrospun Nanofibers as Chemosensors for Detecting Environmental Pollutants: A Review. *Chemosensors* **2023**, *11*, 208. [CrossRef]
2. Cao, X.; Chen, W.; Zhao, P.; Yang, Y.; Yu, D.-G. Electrospun porous nanofibers: Pore–forming mechanisms and applications for photocatalytic degradation of organic pollutants in wastewater. *Polymers* **2022**, *14*, 3390. [CrossRef] [PubMed]
3. Xu, X.; Lv, H.; Zhang, M.; Wang, M.; Zhou, Y.; Liu, Y.; Yu, D.-G. Recent progress in electrospun nanofibers and their applications in heavy metal wastewater treatment. *Front. Chem. Sci. Eng.* **2023**, *17*, 249–275. [CrossRef]
4. Jiang, N.; Shang, R.; Heijman, S.G.J.; Rietveld, L.C. High-silica zeolites for adsorption of organic micro-pollutants in water treatment: A review. *Water. Res.* **2018**, *144*, 145–161. [CrossRef] [PubMed]
5. Vasilachi, I.C.; Asiminicesei, D.M.; Fertu, D.I.; Gavrilescu, M. Occurrence and fate of emerging pollutants in water environment and options for their removal. *Water* **2021**, *13*, 181. [CrossRef]
6. Tan, L.C.; Nancharaiah, Y.V.; Van Hullebusch, E.D.; Lens, P.N.L. Selenium: Environmental significance, pollution, and biological treatment technologies. *Biotechnol. Adv.* **2016**, *34*, 886–907. [CrossRef]
7. Rapti, I.; Boti, V.; Albanis, T.; Konstantinou, I. Photocatalytic degradation of psychiatric pharmaceuticals in hospital WWTP secondary effluents using g-C_3N_4 and g-C_3N_4/MoS_2 catalysts in laboratory-scale pilot. *Catalysts* **2023**, *13*, 252. [CrossRef]
8. Li, D.; Xu, K.; Niu, Z.; Zhang, C. Annealing and plasma effects on the structural and photocatalytic properties of TiO_2 fibers produced by electrospinning. *Catalysts* **2022**, *12*, 1441. [CrossRef]
9. Bairamis, F.; Konstantinou, I.; Petrakis, D.; Vaimakis, T. Enhanced performance of electrospun nanofibrous TiO_2/g-C_3N_4 photocatalyst in photocatalytic degradation of methylene blue. *Catalysts* **2019**, *9*, 880. [CrossRef]
10. Nasir, A.M.; Awang, N.; Jaafar, J.; Ismail, A.F.; Othman, M.H.D.; Rahman, A.M.; Aziz, F.; Mat Yajid, M.A. Recent progress on fabrication and application of electrospun nanofibrous photocatalytic membranes for wastewater treatment: A review. *J. Water Process Eng.* **2021**, *40*, 101878. [CrossRef]
11. Chen, H.; Huang, M.; Liu, Y.; Meng, L.; Ma, M. Functionalized electrospun nanofiber membranes for water treatment: A review. *Sci. Total Environ.* **2020**, *739*, 139944. [CrossRef]
12. Kaneva, N.; Bojinova, A.; Papazova, K. Enhanced removal of organic dyes using co-catalytic Ag-modified ZnO and TiO_2 sol-gel photocatalysts. *Catalysts* **2023**, *13*, 245. [CrossRef]
13. Dutta, D.P.; Abraham, S. Composite of α-FeOOH and mesoporous carbon derived from Indian blackberry seeds as low-cost and recyclable photocatalyst for degradation of ciprofloxacin. *Catalysts* **2023**, *13*, 191. [CrossRef]
14. Zhang, H.; Mane, A.U.; Yang, X.; Xia, Z.; Barry, E.F.; Luo, J.; Wan, Y.; Elam, J.W.; Darling, S.B. Visible-light-activated photocatalytic films toward self-cleaning membranes. *Adv. Funct. Mater.* **2020**, *30*, 2002847. [CrossRef]
15. Yue, Y.; Hou, K.; Chen, J.; Cheng, W.; Wu, Q.; Han, J.; Jiang, J. Ag/AgBr/$AgVO_3$ photocatalyst-embedded polyacrylonitrile/polyamide/chitosan nanofiltration membrane for integrated filtration and degradation of rhb. *ACS Appl. Mater. Inter.* **2022**, *14*, 24708–24719. [CrossRef] [PubMed]
16. Wang, M.; Ge, R.L.; Zhang, F.; Yu, D.G.; Liu, Z.P.; Li, X.; Shen, H.; Williams, G.R. Electrospun Fibers with Blank Surface and Inner Drug Gradient for Improving Sustained Release. *Biomater. Adv.* **2023**, *2*, 213404. [CrossRef]
17. Lee, C.-G.; Javed, H.; Zhang, D.; Kim, J.-H.; Westerhoff, P.; Li, Q.; Alvarez, P.J.J. Porous electrospun fibers embedding TiO_2 for adsorption and photocatalytic degradation of water pollutants. *Environ. Sci. Technol.* **2018**, *52*, 4285–4293. [CrossRef] [PubMed]

18. Joshi, B.N.; Yoon, H.; van Hest, M.F.A.M.; Yoon, S.S. Niobium-doped titania photocatalyst film prepared via a nonaqueous sol-gel method. *J. Am. Ceram. Soc.* **2013**, *96*, 2623–2627. [CrossRef]
19. Wu, W.; Yin, X.; Dai, B.; Kou, J.; Ni, Y.; Lu, C. Water flow drived piezo-photocatalytic flexible films: Bi-piezoelectric integration of ZnO nanorods and PVDF. *Appl. Surf. Sci.* **2020**, *517*, 146119. [CrossRef]
20. Sun, F.; Qi, H.; Xie, Y.; Ma, Q.; He, W.; Xu, D.; Wang, G.; Yu, W.; Wang, T.; Dong, X. Flexible self-supporting bifunctional [TiO_2/C]//[Bi_2WO_6/C] carbon-based Janus nanofiber heterojunction photocatalysts for efficient hydrogen evolution and degradation of organic pollutant. *J. Alloy. Compd.* **2020**, *830*, 154673. [CrossRef]
21. Yao, L.; Sun, C.; Lin, H.; Li, G.; Lian, Z.; Song, R.; Zhuang, S.; Zhang, D. Electrospun Bi-decorated $Bi_xTi_yO_z/TiO_2$ flexible carbon nanofibers and their applications on degradating of organic pollutants under solar radiation. *J. Mater. Sci. Technol.* **2023**, *150*, 114–123. [CrossRef]
22. Sharifi Rad, A.; Afshar, A.; Azadeh, M. Antireflection and photocatalytic single layer and double layer ZnO and ZnO–TiO_2 thin films. *Opt. Mater.* **2023**, *136*, 113501. [CrossRef]
23. Yao, L.; Sun, C.; Lin, H.; Li, G.; Lian, Z.; Song, R.; Zhuang, S.; Zhang, D. Enhancement of AFB1 Removal Efficiency via Adsorption/Photocatalysis Synergy Using Surface-Modifified Electrospun PCL-g-C_3N_4/CQDs Membranes. *Biomolecules* **2023**, *13*, 550. [CrossRef]
24. Li, C.; Yang, J.; He, W.; Xiong, M.; Niu, X.; Li, X.; Yu, D.-G. A review on fabrication and application of tunable hybrid micro–nano array surfaces. *Adv. Mater. Interfaces* **2023**, *10*, 2202160. [CrossRef]
25. Yu, D.-G.; Du, Y.; Chen, J.; Song, W.; Zhou, T. A Correlation Analysis between Undergraduate Students' Safety Behaviors in the Laboratory and Their Learning Efficiencies. *Behav. Sci.* **2023**, *13*, 127. [CrossRef] [PubMed]
26. Kang, S.; Hou, S.; Chen, X.; Yu, D.-G.; Wang, L.; Li, X.; Williams, G.R. Energy-Saving Electrospinning with a Concentric Teflon-Core Rod Spinneret to Create Medicated Nanofibers. *Polymers* **2020**, *12*, 2421. [CrossRef] [PubMed]
27. Liu, H.; Bai, Y.; Huang, C.; Wang, Y.; Ji, Y.; Du, Y.; Xu, L.; Yu, D.-G.; Bligh, S.W. Recent progress of electrospun herbal medicine nanofibers. *Biomolecules* **2023**, *13*, 184. [CrossRef]
28. Zhou, Y.; Wang, M.; Yan, C.; Liu, H.; Yu, D.-G. Advances in the application of electrospun drug-loaded nanofibers in the treatment of oral ulcers. *Biomolecules* **2022**, *12*, 1254. [CrossRef] [PubMed]
29. Huang, X.; Jiang, W.; Zhou, J.; Yu, D.-G.; Liu, H. The applications of ferulic-acid-loaded fibrous films for fruit preservation. *Polymers* **2022**, *14*, 4947. [CrossRef]
30. Wang, Y.; Yu, D.-G.; Liu, Y.; Liu, Y.-N. Progress of electrospun nanofibrous carriers for modifications to drug release profiles. *J. Funct. Biomater.* **2022**, *13*, 289. [CrossRef]
31. Tang, X.; Qi, H.; Yang, L.; Xie, Y.; Ma, Q.; Yu, W.; Dong, X.; Li, D.; Liu, G.; Wang, J. Novel photosensitive dual-anisotropic conductive Janus film endued with magnetic-luminescent properties and derivative 3D structures. *J. Colloid. Interf. Sci.* **2021**, *601*, 899–914. [CrossRef] [PubMed]
32. Xu, J.; Zhong, M.; Song, N.; Wang, C.; Lu, X. General synthesis of Pt and Ni co-doped porous carbon nanofibers to boost HER performance in both acidic and alkaline solutions. *Chin. Chem. Lett.* **2023**, *34*, 107359. [CrossRef]
33. Bai, Y.; Liu, Y.; Lv, H.; Shi, H.; Zhou, W.; Liu, Y.; Yu, D.-G. Processes of electrospun polyvinylidene fluoride-based nanofibers, their piezoelectric properties, and several fantastic applications. *Polymers* **2022**, *14*, 4311. [CrossRef] [PubMed]
34. Yu, D.-G.; Zhao, P. The key elements for biomolecules to biomaterials and to bioapplications. *Biomolecules* **2022**, *12*, 1234. [CrossRef]
35. Shen, Y.; Yu, X.; Cui, J.; Yu, F.; Liu, M.; Chen, Y.; Wu, J.; Sun, B.; Mo, X. Development of biodegradable polymeric stents for the treatment of cardiovascular diseases. *Biomolecules* **2022**, *12*, 1245. [CrossRef]
36. Xie, D.; Zhou, X.; Xiao, B.; Duan, L.; Zhu, Z. Mucus-penetrating silk fibroin-based nanotherapeutics for efficient treatment of ulcerative colitis. *Biomolecules* **2022**, *12*, 1263. [CrossRef]
37. Lakshmi, B.B.; Dorhout, P.K.; Martin, C.R. Sol–gel template synthesis of semiconductor nanostructures. *Chem. Mater.* **1997**, *9*, 857–862. [CrossRef]
38. He, C.-H.; Gong, J. The preparation of PVA–Pt/TiO_2 composite nanofiber aggregate and the photocatalytic degradation of solid-phase polyvinyl alcohol. *Polym. Degrad. Stabil.* **2003**, *81*, 117–124. [CrossRef]
39. Du, Y.; Yang, Z.; Kang, S.; Yu, D.-G.; Chen, X.; Shao, J. A Sequential Electrospinning of a Coaxial and Blending Process for Creating Double-Layer Hybrid Films to Sense Glucose. *Sensors* **2023**, *23*, 3685. [CrossRef]
40. Yu, D.-G.; Li, Q.; Song, W.; Xu, L.; Zhang, K.; Zhou, T. Advanced technique-based combination of innovation education and safety education in higher education. *J. Chem. Educ.* **2023**, *100*, 507–516. [CrossRef]
41. Song, W.; Tang, Y.; Qian, C.; Kim, B.J.; Liao, Y.; Yu, D.-G. Electrospinning spinneret: A bridge between the visible world and the invisible nanostructures. *Innovation* **2023**, *4*, 100381. [CrossRef] [PubMed]
42. Sun, F.; Qi, H.; Xie, Y.; Xu, D.; Yu, W.; Ma, Q.; Yang, Y.; Yu, H.; Dong, X. Self-standing Janus nanofiber heterostructure photocatalyst with hydrogen production and degradation of methylene blue. *J. Am. Ceram. Soc.* **2022**, *105*, 1428–1441. [CrossRef]
43. Jirkovec, R.; Holec, P.; Hauzerova, S.; Samkova, A.; Kalous, T.; Chvojka, J. Preparation of a composite scaffold from polycaprolactone and hydroxyapatite particles by means of alternating current electrospinning. *ACS Omega* **2021**, *6*, 9234–9242. [CrossRef] [PubMed]
44. Li, Z.; Lei, I.M.; Davoodi, P.; Huleihel, L.; Huang, Y.Y.S. Solution formulation and rheology for fabricating extracellular matrix-derived fibers using low-voltage electrospinning patterning. *ACS Biomater. Sci. Eng.* **2019**, *5*, 3676–3684. [CrossRef]

45. Deng, J.; Kang, X.; Chen, L.; Wang, Y.; Gu, Z.; Lu, Z. A nanofiber functionalized with dithizone by co-electrospinning for lead (II) adsorption from aqueous media. *J. Hazard. Mater.* **2011**, *196*, 187–193. [CrossRef]
46. Yin, J.; Bai, Y.; Lu, J.; Ma, J.; Zhang, Q.; Hong, W.; Jiao, T. Enhanced mechanical performances and high-conductivity of rGO/PEDOT:PSS/PVA composite fiber films via electrospinning strategy. *Colloid. Surf. A* **2022**, *643*, 128791. [CrossRef]
47. Smit, E.; Bűttner, U.; Sanderson, R.D. Continuous yarns from electrospun fibers. *Polymer* **2005**, *46*, 2419–2423. [CrossRef]
48. Haghi, A.K.; Akbari, M. Trends in electrospinning of natural nanofibers. *Phys. Status Solidi A* **2007**, *204*, 1830–1834. [CrossRef]
49. Valizadeh, A.; Mussa Farkhani, S. Electrospinning and electrospun nanofibres. *IET Nanobiotechnol.* **2014**, *8*, 83–92. [CrossRef]
50. Han, W.; Wang, L.; Li, Q.; Ma, B.; He, C.; Guo, X.; Nie, J.; Ma, G. A review: Current status and emerging developments on natural polymer-based electrospun fibers. *Macromol. Rapid Comm.* **2022**, *43*, 2200456. [CrossRef]
51. Wang, M.-L.; Yu, D.-G.; Annie Bligh, S.W. Progress in Preparing Electrospun Janus Fibers and Their Applications. *App. Mater. Today* **2023**, *31*, 101766. [CrossRef]
52. Shen, M.; Liu, H.; Pan, T.; Ning, J.; Zhou, D.; Song, G.; Wang, Y.; Cai, S.; Xia, X.; Zhang, G.; et al. Crosslinked PVA electrospinning nanofibrous film as a new platform for the design of K^+ sensor. *Sens. Actuators B-Chem.* **2023**, *380*, 133317. [CrossRef]
53. Yogeswari, C.; Hijas, K.M.; Sabari Girisun, T.C.; Nagalakshmi, R. Synthesis of nanoscale 4-nitroaniline-polystyrene fiber for optical limiting application using electrospinning technique. *Mater. Today Proc.* **2021**, *39*, 1719–1721. [CrossRef]
54. Wang, M.; Hou, J.; Yu, D.-G.; Li, S.; Zhu, J.; Chen, Z. Electrospun tri-layer nanodepots for sustained release of acyclovir. *J. Alloy. Compd.* **2020**, *846*, 156471. [CrossRef]
55. Matthews, J.A.; Wnek, G.E.; Simpson, D.G.; Bowlin, G.L. Electrospinning of collagen nanofibers. *Biomacromolecules* **2002**, *3*, 232–238. [CrossRef]
56. Zhou, H.; Green, T.B.; Joo, Y.L. The thermal effects on electrospinning of polylactic acid melts. *Polymer* **2006**, *47*, 7497–7505. [CrossRef]
57. Xu, H.; Zhang, F.; Wang, M.; Lv, H.; Yu, D.-G.; Liu, X.; Shen, H. Electrospun hierarchical structural films for effective wound healing. *Biomater. Adv.* **2022**, *136*, 212795. [CrossRef] [PubMed]
58. Schiffman, J.D.; Stulga, L.A.; Schauer, C.L. Chitin and chitosan: Transformations due to the electrospinning process. *Polym. Eng. Sci.* **2009**, *49*, 1918–1928. [CrossRef]
59. Fang, D.; Liu, Y.; Jiang, S.; Nie, J.; Ma, G. Effect of intermolecular interaction on electrospinning of sodium alginate. *Carbohyd. Polym.* **2011**, *85*, 276–279. [CrossRef]
60. Rezabeigi, E.; Sta, M.; Swain, M.; McDonald, J.; Demarquette, N.R.; Drew, R.A.L.; Wood-Adams, P.M. Electrospinning of porous polylactic acid fibers during nonsolvent induced phase separation. *J. Appl. Polym. Sci.* **2017**, *134*, 44862. [CrossRef]
61. Zavgorodnya, O.; Shamshina, J.L.; Bonner, J.R.; Rogers, R.D. Electrospinning biopolymers from ionic liquids requires control of different solution properties than volatile organic solvents. *ACS Sustain. Chem. Eng.* **2017**, *5*, 5512–5519. [CrossRef]
62. Chuangchote, S.; Sagawa, T.; Yoshikawa, S. Electrospinning of poly(vinyl pyrrolidone): Effects of solvents on electrospinnability for the fabrication of poly(p-phenylene vinylene) and TiO_2 nanofibers. *J. Appl. Polym. Sci.* **2009**, *114*, 2777–2791. [CrossRef]
63. Alipour, S.M.; Nouri, M.; Mokhtari, J.; Bahrami, S.H. Electrospinning of poly(vinyl alcohol)–water-soluble quaternized chitosan derivative blend. *Carbohyd. Res.* **2009**, *344*, 2496–2501. [CrossRef]
64. Chapman, B.S.; Mishra, S.R.; Tracy, J.B. Direct electrospinning of titania nanofibers with ethanol. *Dalton Trans.* **2019**, *48*, 12822–12827. [CrossRef] [PubMed]
65. Lv, H.; Liu, Y.; Zhao, P.; Bai, Y.; Cui, W.; Shen, S.; Liu, Y.; Wang, Z.; Yu, D.-G. Insight into the superior piezophotocatalytic performance of $BaTiO_3$//ZnO Janus nanofibrous heterostructures in the treatment of multi-pollutants from water. *Appl. Catal. B-Environ.* **2023**, *330*, 122623. [CrossRef]
66. Wang, P.; Lv, H.; Cao, X.; Liu, Y.; Yu, D.-G. Recent Progress of the Preparation and Application of Electrospun Porous Nanofibers. *Polymers* **2023**, *15*, 921. [CrossRef]
67. Liu, H.; Dai, Y.; Li, J.; Liu, P.; Zhou, W.; Yu, D.G.; Ge, R. Safe, Fast and Convenient Delivery of Fluidextracts Liquorice through Electrospun Core-Shell Nanohybrids. *Front. Bioeng. Biotechnol.* **2023**, *11*, 1172133. [CrossRef]
68. De Vrieze, S.; Van Camp, T.; Nelvig, A.; Hagström, B.; Westbroek, P.; De Clerck, K. The effect of temperature and humidity on electrospinning. *J. Mater. Sci.* **2009**, *44*, 1357–1362. [CrossRef]
69. Pelipenko, J.; Kristl, J.; Janković, B.; Baumgartner, S.; Kocbek, P. The impact of relative humidity during electrospinning on the morphology and mechanical properties of nanofibers. *Int. J. Pharmaceut.* **2013**, *456*, 125–134. [CrossRef]
70. Deitzel, J.M.; Kleinmeyer, J.; Harris, D.; Beck Tan, N.C. The effect of processing variables on the morphology of electrospun nanofibers and textiles. *Polymer* **2001**, *42*, 261–272. [CrossRef]
71. Lv, H.; Guo, S.; Zhang, G.; He, W.; Wu, Y.; Yu, D.-G. Electrospun structural hybrids of acyclovir-polyacrylonitrile at acyclovir for modifying drug release. *Polymers* **2021**, *13*, 4286. [CrossRef] [PubMed]
72. Ge, R.; Ji, Y.; Ding, Y.; Huang, C.; He, H.; Yu, D.-G. Electrospun self-emulsifying core-shell nanofibers for effective delivery of paclitaxel. *Front. Bioeng. Biotechnol.* **2023**, *11*, 1112338. [CrossRef] [PubMed]
73. Bi, F.; Dong, X.; Wang, J.; Liu, G. Tuned magnetism–luminescence bifunctionality simultaneously assembled into flexible Janus nanofiber. *RSC Adv.* **2015**, *5*, 12571–12577. [CrossRef]
74. Tucker, N.; Stanger, J.J.; Staiger, M.P.; Razzaq, H.; Hofman, K. The history of the science and technology of electrospinning from 1600 to 1995. *J. Eng. Fiber. Fabr.* **2012**, *7*, 155892501200702. [CrossRef]

75. Liu, X.; Xie, Y.; Yang, L.; Qi, H.; Ma, Q.; Dong, X.; Li, D.; Liu, G.; Wang, J.; Yu, W. Tricolor flag-shaped nanobelt array and derivant 3D structures display concurrent conductive anisotropy, up-conversion fluorescence and magnetism. *Mater. Des.* **2021**, *211*, 110121. [CrossRef]
76. Feng, Z.; Wang, K.; Liu, Y.; Han, B.; Yu, D.-G. Piezoelectric Enhancement of Piezoceramic Nanoparticle-Doped PVDF/PCL Core-Sheath Fibers. *Nanomaterials* **2023**, *13*, 1243. [CrossRef]
77. Xi, X.; Yu, W.; Li, D.; Ma, Q.; Dong, X.; Wang, J.; Liu, G. Employing novel Janus nanobelts to achieve anisotropic conductive array pellicle functionalized by superparamagnetism and green fluorescence. *J. Mater. Sci.-Mater. El.* **2019**, *30*, 4219–4230. [CrossRef]
78. Mohamed, A.; Ghobara, M.M.; Abdelmaksoud, M.K.; Mohamed, G.G. A novel and highly efficient photocatalytic degradation of malachite green dye via surface modified polyacrylonitrile nanofibers/biogenic silica composite nanofibers. *Sep. Purif. Technol.* **2019**, *210*, 935–942. [CrossRef]
79. Yi, S.; Sun, S.; Zhang, Y.; Zou, Y.; Dai, F.; Si, Y. Scalable fabrication of bimetal modified polyacrylonitrile (PAN) nanofibrous membranes for photocatalytic degradation of dyes. *J. Colloid. Interf. Sci.* **2020**, *559*, 134–142. [CrossRef] [PubMed]
80. Li, F.; Dong, Y.; Kang, W.; Cheng, B.; Cui, G. Enhanced removal of azo dye using modified PAN nanofibrous membrane Fe complexes with adsorption/visible-driven photocatalysis bifunctional roles. *Appl. Surf. Sci.* **2017**, *404*, 206–215. [CrossRef]
81. Uheida, A.; Mohamed, A.; Belaqziz, M.; Nasser, W.S. Photocatalytic degradation of Ibuprofen, Naproxen, and Cetirizine using PAN-MWCNT nanofibers crosslinked TiO_2-NH_2 nanoparticles under visible light irradiation. *Sep. Purif. Technol.* **2019**, *212*, 110–118. [CrossRef]
82. Elkady, M.F.; Hassan, H.S. Photocatalytic degradation of malachite green dye from aqueous solution using environmentally compatible Ag/ZnO polymeric nanofibers. *Polymers* **2021**, *13*, 2033. [CrossRef] [PubMed]
83. Lv, H.; Zhang, M.; Wang, P.; Xu, X.; Liu, Y.; Yu, D.-G. Ingenious construction of $Ni(DMG)_2/TiO_2$-decorated porous nanofibers for the highly efficient photodegradation of pollutants in water. *Colloids Surf. A* **2022**, *650*, 129561. [CrossRef]
84. Wu, H.; Xu, L.; Jia, J.; Dong, F.; Jia, Y.; Liu, X. In situ electrospun porous MIL-88A/PAN nanofibrous membranes for efficient removal of organic dyes. *Molecules* **2023**, *28*, 760. [CrossRef] [PubMed]
85. Liu, Y.; Wang, M.; Li, Z.; Liu, H.; He, P.; Li, J. Preparation of porous aminopropylsilsesquioxane by a nonhydrolytic sol–gel method in ionic liquid solvent. *Langmuir* **2005**, *21*, 1618–1622. [CrossRef]
86. Dutta, T.; Kim, T.; Vellingiri, K.; Tsang, D.C.W.; Shon, J.R.; Kim, K.-H.; Kumar, S. Recycling and regeneration of carbonaceous and porous materials through thermal or solvent treatment. *Chem. Eng. J.* **2019**, *364*, 514–529. [CrossRef]
87. Habib, Z.; Lee, C.-G.; Li, Q.; Khan, S.J.; Ahmad, N.M.; Jamal, Y.; Huang, X.; Javed, H. Bi-polymer electrospun nanofibers embedding Ag_3PO_4/P25 composite for efficient photocatalytic degradation and anti-microbial activity. *Catalysts* **2020**, *10*, 784. [CrossRef]
88. Machida, S.; Katsumata, K.; Yasumori, A. A stable layered inorganic solid at high temperature: Heat treatment of Eu-doped hexacelsian without phase transformation. *J. Solid State Chem.* **2023**, *322*, 123945. [CrossRef]
89. Sun, C.; Dai, L.; He, X.; Liu, F.; Yuan, F.; Gao, Y. Effect of heat treatment on physical, structural, thermal and morphological characteristics of zein in ethanol-water solution. *Food Hydrocolloid.* **2016**, *58*, 11–19. [CrossRef]
90. Sun, C.; Dai, L.; Liu, F.; Gao, Y. Simultaneous treatment of heat and high pressure homogenization of zein in ethanol–water solution: Physical, structural, thermal and morphological characteristics. *Innov. Food Sci. Emerg.* **2016**, *34*, 161–170. [CrossRef]
91. Swanckaert, B.; Geltmeyer, J.; Rabaey, K.; De Buysser, K.; Bonin, L.; De Clerck, K. A review on ion-exchange nanofiber membranes: Properties, structure and application in electrochemical (waste)water treatment. *Sep. Purif. Technol.* **2022**, *287*, 120529. [CrossRef]
92. Kalashnikov, I.S.; Acselrad, O.; Shalkevich, A.; Chumakova, L.D.; Pereira, L.C. Heat treatment and thermal stability of FeMnAlC alloys. *J. Mater. Process. Tech.* **2003**, *136*, 72–79. [CrossRef]
93. Gao, J.; Qiao, L.; Li, L.; Wang, Y. Hemolysis effect and calcium-phosphate precipitation of heat-organic-film treated magnesium. *Trans. Nonferrous Met. Soc. China* **2006**, *16*, 539–544. [CrossRef]
94. Singh, P.; Mondal, K.; Sharma, A. Reusable electrospun mesoporous ZnO nanofiber mats for photocatalytic degradation of polycyclic aromatic hydrocarbon dyes in wastewater. *J. Colloid. Interf. Sci.* **2013**, *394*, 208–215. [CrossRef]
95. Norouzi, M.; Fazeli, A.; Tavakoli, O. Photocatalytic degradation of phenol under visible light using electrospun Ag/TiO_2 as a 2D nano-powder: Optimizing calcination temperature and promoter content. *Adv. Powder Technol.* **2022**, *33*, 103792. [CrossRef]
96. Zaborowska, M.; Smok, W.; Tański, T. Electrospinning synthesis and characterization of zirconia nanofibers annealed at different temperatures. *Appl. Surf. Sci.* **2023**, *615*, 156342. [CrossRef]
97. Song, M.; Cao, H.; Zhu, Y.; Wang, Y.; Zhao, S.; Huang, C.; Zhang, C.; He, X. Electrochemical and photocatalytic properties of electrospun C/TiO_2 nanofibers. *Chem. Phys. Lett.* **2020**, *747*, 137355. [CrossRef]
98. Zhai, G.; Zhou, J.; Xie, M.; Jia, C.; Hu, Z.; Xiang, H.; Zhu, M. Improved photocatalytic property of lignin-derived carbon nanofibers through catalyst synergy. *Int. J. Biol. Macromol.* **2023**, *233*, 123588. [CrossRef] [PubMed]
99. Zhao, Y.; Nie, L.; Yang, H.; Song, K.; Hou, H. Tailored fabrication of TiO_2/In_2O_3 hybrid mesoporous nanofibers towards enhanced photocatalytic performance. *Colloids Surf. A* **2021**, *629*, 127455. [CrossRef]
100. Ramos, P.G.; Flores, E.; Luyo, C.; Sánchez, L.A.; Rodriguez, J. Fabrication of ZnO-RGO nanorods by electrospinning assisted hydrothermal method with enhanced photocatalytic activity. *Mater. Today Commun.* **2019**, *19*, 407–412. [CrossRef]
101. Zhou, M.; Zou, W.; Zhu, X.; Ma, H.; Wang, P.; Shang, J.; Luo, P. In situ growth of UIO-66-NH_2 on thermally stabilized electrospun polyacrylonitrile nanofibers for visible-light driven Cr(VI) photocatalytic reduction. *J. Solid State Chem.* **2022**, *307*, 122836. [CrossRef]

102. Sharma, J.; Sharma, S.; Soni, V. Classification and impact of synthetic textile dyes on Aquatic Flora: A review. *Reg. Stud. Mar. Sci.* **2021**, *45*, 101802. [CrossRef]
103. Al-Tohamy, R.; Ali, S.S.; Li, F.; Okasha, K.M.; Mahmoud, Y.A.-G.; Elsamahy, T.; Jiao, H.; Fu, Y.; Sun, J. A critical review on the treatment of dye-containing wastewater: Ecotoxicological and health concerns of textile dyes and possible remediation approaches for environmental safety. *Ecotoxicol. Environ. Saf.* **2022**, *231*, 113160. [CrossRef] [PubMed]
104. Rauf, M.A.; Ashraf, S.S. Fundamental principles and application of heterogeneous photocatalytic degradation of dyes in solution. *Chem. Eng. J.* **2009**, *151*, 10–18. [CrossRef]
105. Zhou, T.; Zhao, L.; Wu, D.; Feng, Q.; Zhao, B. Uniformly assembled polypyrrole-covered bacterial cellulose/g-C_3N_4 flexible nanofiber membrane for catalytic degradation of tetracycline hydrochloride. *J. Water Process Eng.* **2022**, *47*, 102775. [CrossRef]
106. Tang, Y.; Fu, S.; Zhao, K.; Teng, L.; Xie, G. Fabrication of TiO_2 micro-/nano-spheres embedded in nanofibers by coaxial electrospinning. *Mater. Res. Bull.* **2016**, *78*, 11–15. [CrossRef]
107. Methaapanon, R.; Chutchakul, K.; Pavarajarn, V. Photocatalytic zinc oxide on flexible polyacrylonitrile nanofibers via sol–gel coaxial electrospinning. *Ceram. Int.* **2020**, *46*, 8287–8292. [CrossRef]
108. Chang, W.; Xu, F.; Mu, X.; Ji, L.; Ma, G.; Nie, J. Fabrication of nanostructured hollow TiO_2 nanofibers with enhanced photocatalytic activity by coaxial electrospinning. *Mater. Res. Bull.* **2013**, *48*, 2661–2668. [CrossRef]
109. Peng, X.; Santulli, A.C.; Sutter, E.; Wong, S.S. Fabrication and enhanced photocatalytic activity of inorganic core–shell nanofibers produced by coaxial electrospinning. *Chem. Sci.* **2012**, *3*, 1262–1272. [CrossRef]
110. Ji, S.M.; Tiwari, A.P.; Kim, H.Y. PAN-ZnO//PAN-Mn_3O_4/CeO_2 Janus nanofibers: Controlled fabrication and enhanced photocatalytic properties under UV and visible light. *Chem. Phys. Lett.* **2020**, *759*, 138050. [CrossRef]
111. Van, T.T.H.; Yidana, Z.; Smooker, P.M.; Coloe, P.J. Antibiotic use in food animals worldwide, with a focus on Africa: Pluses and minuses. *J. Glob. Antimicrob. Resist.* **2020**, *20*, 170–177. [CrossRef]
112. Park, Y.; Kim, S.; Kim, J.; Khan, S.; Han, C. UV/TiO_2 photocatalysis as an efficient livestock wastewater quaternary treatment for antibiotics removal. *Water* **2022**, *14*, 958. [CrossRef]
113. Yin, H.; Li, G.; Chen, X.; Wang, W.; Wong, P.K.; Zhao, H.; An, T. Accelerated evolution of bacterial antibiotic resistance through early emerged stress responses driven by photocatalytic oxidation. *Appl. Catal. B-Environ.* **2020**, *269*, 118829. [CrossRef]
114. Li, W.; Li, T.; Li, G.; An, L.; Li, F.; Zhang, Z. Electrospun $H_4SiW_{12}O_{40}$/cellulose acetate composite nanofibrous membrane for photocatalytic degradation of tetracycline and methyl orange with different mechanism. *Carbohydr. Polym.* **2017**, *168*, 153–162. [CrossRef] [PubMed]
115. Zhang, J.-J.; Kai, C.-M.; Zhang, F.-J.; Wang, Y.-R. Novel PAN/Bi_2MoO_6/Ti_3C_2 ternary composite membrane via electrospinning with enhanced photocatalytic degradation of tetracycline. *Colloids Surf. A* **2022**, *648*, 129255. [CrossRef]
116. Wang, B.; Cao, Q.; Cheng, M.; Li, G.; Zhang, J.; Jiang, H. Photocatalytic degradation of antibiotics in water by pollution-free photocatalytic films with a three-dimensional layered structure and the reaction mechanism study. *J. Water Process Eng.* **2023**, *52*, 103550. [CrossRef]
117. Zhang, L.; Shen, Q.; Huang, F.; Jiang, L.; Liu, J.; Sheng, J.; Li, Y.; Yang, H. Electrospinning directly synthesis of 0D/1D $CuBi_2O_4$@WO_3 nanofiber photocatalyst with S-scheme heterojunction. *Appl. Surf. Sci.* **2023**, *608*, 155064. [CrossRef]
118. Li, X. Technical solutions for the safe utilization of heavy metal-contaminated farmland in China: A critical review. *Land Degrad. Dev.* **2019**, *30*, 1773–1784. [CrossRef]
119. Mitra, S.; Chakraborty, A.J.; Tareq, A.M.; Emran, T.B.; Nainu, F.; Khusro, A.; Idris, A.M.; Khandaker, M.U.; Osman, H.; Alhumaydhi, F.A.; et al. Impact of heavy metals on the environment and human health: Novel therapeutic insights to counter the toxicity. *J. King Saud. Univ. Sci.* **2022**, *34*, 101865. [CrossRef]
120. Li, Z.; Wang, L.; Qin, L.; Lai, C.; Wang, Z.; Zhou, M.; Xiao, L.; Liu, S.; Zhang, M. Recent advances in the application of water-stable metal-organic frameworks: Adsorption and photocatalytic reduction of heavy metal in water. *Chemosphere* **2021**, *285*, 131432. [CrossRef]
121. Gu, D.; Liu, Y.; Li, X.; Zhu, H.; Cui, Y.; Yang, W.; Hao, J. Porphyrin-based metal–organic frameworks loaded with Ag nanoparticles and their nanofibrous filters for the photocatalytic reduction of Cr(VI). *Appl. Surf. Sci.* **2023**, *614*, 156192. [CrossRef]
122. Lu, W.; Duan, C.; Zhang, Y.; Gao, K.; Dai, L.; Shen, M.; Wang, W.; Wang, J.; Ni, Y. Cellulose-based electrospun nanofiber membrane with core-sheath structure and robust photocatalytic activity for simultaneous and efficient oil emulsions separation, dye degradation and Cr(VI) reduction. *Carbohydr. Polym.* **2021**, *258*, 117676. [CrossRef] [PubMed]
123. Imran, M.; Das, K.R.; Naik, M.M. Co-selection of multi-antibiotic resistance in bacterial pathogens in metal and microplastic contaminated environments: An emerging health threat. *Chemosphere* **2019**, *215*, 846–857. [CrossRef]
124. Baaloudj, O.; Assadi, I.; Nasrallah, N.; El Jery, A.; Khezami, L.; Assadi, A.A. Simultaneous removal of antibiotics and inactivation of antibiotic-resistant bacteria by photocatalysis: A review. *J. Water Process Eng.* **2021**, *42*, 102089. [CrossRef]
125. Ademola Bode-Aluko, C.; Pereao, O.; Kyaw, H.H.; Al-Naamani, L.; Al-Abri, M.Z.; Tay Zar Myint, M.; Rossouw, A.; Fatoba, O.; Petrik, L.; Dobretsov, S. Photocatalytic and antifouling properties of electrospun TiO_2 polyacrylonitrile composite nanofibers under visible light. *Mater. Sci. Eng. B-Adv.* **2021**, *264*, 114913. [CrossRef]
126. Yerli-Soylu, N.; Akturk, A.; Kabak, Ö.; Erol-Taygun, M.; Karbancioglu-Guler, F.; Küçükbayrak, S. TiO_2 nanocomposite ceramics doped with silver nanoparticles for the photocatalytic degradation of methylene blue and antibacterial activity against Escherichia coli. *Eng. Sci. Technol.* **2022**, *35*, 101175. [CrossRef]

127. Wang, L.; Ali, J.; Zhang, C.; Mailhot, G.; Pan, G. Simultaneously enhanced photocatalytic and antibacterial activities of TiO_2/Ag composite nanofibers for wastewater purification. *J. Environ. Chem. Eng.* **2020**, *8*, 102104. [CrossRef]
128. Van-Pham, D.-T.; Thi Yen Nhi, P.; Vu Bao Long, T.; Nguyen, C.-N.; Minh Nhan, L.; Thi Bich Quyen, T.; Thi Cam Tuyen, L.; Truong Ngoc Mai, N.; Van Hong Thien, D. Electrospun Fe-doped TiO_2/chitosan/PVA nanofibers: Preparation and study on photocatalytic and adsorption properties. *Mater. Lett.* **2022**, *326*, 132930. [CrossRef]
129. Sarkodie, B.; Amesimeku, J.; Frimpong, C.; Howard, E.K.; Feng, Q.; Xu, Z. Photocatalytic degradation of dyes by novel electrospun nanofibers: A review. *Chemosphere* **2023**, *313*, 137654. [CrossRef]
130. Asgari, S.; Mohammadi Ziarani, G.; Badiei, A.; Setayeshmehr, M.; Kiani, M.; Pourjavadi, A. Electrospun Ag-decorated reduced GO-graft-chitosan composite nanofibers with visible light photocatalytic activity for antibacterial performance. *Chemosphere* **2022**, *299*, 134436. [CrossRef]
131. Khademi, D.; Zargazi, M.; Chahkandi, M.; Baghayeri, M. A novel γ–BMO@BMWO Z–Scheme heterojunction for promotion photocatalytic performance: Nanofibers thin film by co–axial–electrospun. *Environ. Res.* **2023**, *219*, 115154. [CrossRef]
132. Qi, W.; Yang, Y.; Du, J.; Yang, J.; Guo, L.; Zhao, L. Highly photocatalytic electrospun Zr/Ag co-doped titanium dioxide nanofibers for degradation of dye. *J. Colloid Interf. Sci.* **2021**, *603*, 594–603. [CrossRef]
133. Pascariu, P.; Cojocaru, C.; Samoila, P.; Olaru, N.; Bele, A.; Airinei, A. Novel electrospun membranes based on PVDF fibers embedding lanthanide doped ZnO for adsorption and photocatalytic degradation of dye organic pollutants. *Mater. Res. Bull.* **2021**, *141*, 111376. [CrossRef]
134. Wang, D.; Yue, Y.; Wang, Q.; Cheng, W.; Han, G. Preparation of cellulose acetate-polyacrylonitrile composite nanofibers by multi-fluid mixing electrospinning method: Morphology, wettability, and mechanical properties. *Appl. Surf. Sci.* **2020**, *510*, 145462. [CrossRef]
135. Zhang, X.; Xie, L.; Wang, X.; Shao, Z.; Kong, B. Electrospinning super-assembly of ultrathin fibers from single- to multi-Taylor cone sites. *Appl. Mater. Today* **2022**, *26*, 101272. [CrossRef]
136. Zhao, T.; Zheng, Y.; Zhang, X.; Teng, D.; Xu, Y.; Zeng, Y. Design of helical groove/hollow nanofibers via tri-fluid electrospinning. *Mater. Des.* **2021**, *205*, 109705. [CrossRef]
137. Li, D.; Yue, G.; Li, S.; Liu, J.; Li, H.; Gao, Y.; Liu, J.; Hou, L.; Liu, X.; Cui, Z.; et al. Fabrication and applications of multi-fluidic electrospinning multi-structure hollow and core–shell nanofibers. *Engineering* **2022**, *13*, 116–127. [CrossRef]
138. Wang, M.; Ge, R.; Zhao, P.; Williams, G.R.; Yu, D.-G.; Bligh, S.W.A. Exploring wettability difference-driven wetting by utilizing electrospun chimeric Janus microfiber comprising cellulose acetate and polyvinylpyrrolidone. *Mater. Des.* **2023**, *226*, 111652. [CrossRef]
139. Huang, H.; Song, Y.; Zhang, Y.; Li, Y.; Li, J.; Lu, X.; Wang, C. Electrospun nanofibers: Current progress and applications in food systems. *J. Agric. Food Chem.* **2022**, *70*, 1391–1409. [CrossRef]
140. Lu, H.; Zhao, Y.; Qin, S.; Zhang, Y.; Liu, J.; Zhang, J.; Feng, C.; Zhao, W. Fluorine substitution tunes the nanofiber chirality of supramolecular hydrogels to promote cell adhesion and proliferation. *Adv. Fiber Mater.* **2023**, *5*, 377–387. [CrossRef]
141. Sun, Z.; Liu, T.; Shen, Q.; Li, H.; Liu, X.; Jia, H.; Xue, J. Synergetic effect of oxygen vacancies coupled with in-situ Bi clusters in Bi_2WO_6 for enhancing photocatalytic CO_2 reduction. *Appl. Surf. Sci.* **2023**, *616*, 156530. [CrossRef]
142. Guo, N.; Cao, X.; Li, Q.; Han, Y.; Li, H.; Yuan, Y. Oxygen-vacancy-rich Ag/Bi_5O_7Br nanosheets enable improved photocatalytic no removal and oxygen evolution under visible light exposure. *Adv. Powder Technol.* **2023**, *34*, 103927. [CrossRef]
143. Reddy, N.R.; Reddy, P.M.; Jyothi, N.; Kumar, A.S.; Jung, J.H.; Joo, S.W. Versatile TiO_2 bandgap modification with metal, non-metal, noble metal, carbon material, and semiconductor for the photoelectrochemical water splitting and photocatalytic dye degradation performance. *J. Alloy Compd.* **2023**, *935*, 167713. [CrossRef]
144. Liu, Q.; Fan, Z.; Yi, X.; Chen, S.; Li, B.; Luo, W. Porous polyimide/carbon quantum dots/ZnS quantum dots material aerogel for efficient visible-light photocatalytic degradation over oxytetracycline. *React. Funct. Polym.* **2022**, *178*, 105330. [CrossRef]
145. Bashir, S.; Jamil, A.; Alazmi, A.; Khan, M.S.; Alsafari, I.A.; Shahid, M. Synergistic effects of doping, composite formation, and nanotechnology to enhance the photocatalytic activities of semiconductive materials. *Opt. Mater.* **2023**, *135*, 113264. [CrossRef]
146. Bashir, S.; Jamil, A.; Amin, R.; Ul-hasan, I.; Alazmi, A.; Shahid, M. Hydrothermally synthesized Gd-doped $BiSbO_4$ nanoparticles and their graphene-based composite: A novel photocatalytic material. *J. Solid State Chem.* **2022**, *312*, 123217. [CrossRef]
147. Zhang, H.; Yin, F.; Shang, S.; Li, Y.; Qiu, Z.; Lin, Q.; Wei, X.; Li, S.; Kim, N.Y.; Shen, G. A high-performance, biocompatible, and degradable piezoresistive-triboelectric hybrid device for cross-scale human activities monitoring and self-powered smart home system. *Nano Energy* **2022**, *102*, 107687. [CrossRef]
148. Zhao, W.; Zheng, J.; Han, C.; Jun, R.; Lu, Y.; Zhou, K.; Zhai, T.; Wang, H.; Yan, H. MnO_x-PMMA self-powered triboelectric catalysts based on three-dimensional nanocomposite structures for formaldehyde degradation at room temperature. *Chem. Eng. J.* **2022**, *440*, 135877. [CrossRef]
149. Zhu, Y.; Zhao, W.; Jing, B.; Zhou, J.; Cai, B.; Li, D.; Ao, Z. Density functional theory calculations on 2H-MoS_2 monolayer for HCHO degradation: Piezoelectric-photocatalytic synergy. *Chin. Chem. Lett.* **2023**, *34*, 107816. [CrossRef]
150. Liu, L.; Zhong, S.; Zhang, L.; Liu, B.; Wang, W. Ti doped BiOCl nanowires for piezoelectric photocatalytic degradation of organic pollutants. *Catal. Commun.* **2022**, *170*, 106493. [CrossRef]
151. Song, W.; Zhang, M.; Huang, X.; Chen, B.; Ding, Y.; Zhang, Y.; Yu, D.-G.; Kim, I. Smart l-borneol-loaded hierarchical hollow polymer nanospheres with antipollution and antibacterial capabilities. *Mater. Today Chem.* **2022**, *26*, 101252. [CrossRef]

152. Li, H.; Zhang, Z.; Ren, Z.; Chen, Y.; Huang, J.; Lei, Z.; Qian, X.; Lai, Y.; Zhang, S. A quadruple biomimetic hydrophilic/hydrophobic Janus composite material integrating $Cu(OH)_2$ micro-needles and embedded bead-on-string nanofiber membrane for efficient fog harvesting. *Chem. Eng. J.* **2023**, *455*, 140863. [CrossRef]
153. Zhao, P.; Li, H.; Bu, W. A forward vision for chemodynamic therapy: Issues and opportunities. *Angew. Chem. Int. Ed.* **2023**, *62*, e202210415. [CrossRef]
154. Meng, Y.; Chen, L.; Chen, Y.; Shi, J.; Zhang, Z.; Wang, Y.; Wu, F.; Jiang, X.; Yang, W.; Zhang, L.; et al. Reactive metal boride nanoparticles trap lipopolysaccharide and peptidoglycan for bacteria-infected wound healing. *Nat. Commun.* **2022**, *13*, 7353. [CrossRef]
155. Wu, Y.; Li, Y.; Lv, G.; Bu, W. Redox dyshomeostasis strategy for tumor therapy based on nanomaterials chemistry. *Chem. Sci.* **2022**, *13*, 2202–2217. [CrossRef] [PubMed]
156. Wang, Q.; Liu, Q.; Gao, J.; He, J.; Zhang, H.; Ding, J. Stereo coverage and overall stiffness of biomaterial arrays underly parts of topography effects on cell adhesion. *ACS Appl. Mater. Inter.* **2023**, *15*, 6142–6155. [CrossRef]
157. Li, C.; Wang, J.; Deng, C.; Wang, R.; Zhang, H. Protocol for atmospheric water harvesting using in situ polymerization honeycomb hygroscopic polymers. *STAR Protoc.* **2022**, *3*, 101780. [CrossRef]